DESIGN OF DONOR-ACCEPTOR CONJUGATED POLYMERS FOR HIGH-PERFORMANCE ORGANIC SOLAR CELLS: A QUANTUM MECHANICAL APPROACH

by

Deniz Ersoy

B.S., Physics, Boğaziçi University, 2013

Submitted to the Institute for Graduate Studies in
Science and Engineering in partial fulfillment of
the requirements for the degree of
Master of Science

Graduate Program in Computational Science and Engineering

Boğaziçi University

2019

ACKNOWLEDGEMENTS

First and most of all, I would like to express my deepest respect and appreciation to my thesis supervisor, Prof. Viktorya Aviyente who has been my mentor and source of motivation from the very first day through her generous support, guidance and understanding towards me. Her trust in me and pushing me to aim for the best kept me motivated through my master's. Her instructions have had significant contributions towards the completion of this study. It has been a great chance studying with her.

I would like to express my sincere gratitude to my thesis advisor, Prof. Levent Kurnaz for his valuable support and guidance through my thesis project.

I would like to gratefully acknowledge H. Taylan Turan and Oğuzhan Kuçur from my lab for assisting me through my studies and answering my questions anytime I needed an answer. I would like to thank them for their kindness and support when I needed any assistance.

I would like to thank my current teammates and manager from Migros and my former teammates and managers from Hepsiburada, Digitouch, Havas Media and GroupM for their understanding towards the lecture hours of my master's which conflict with working hours.

I would also like to thank my lovely people Bahar Üğütücü, Eda Nur Pilav, Gözde Bumin, İlay Çokyiğit, İrem Esen, Melih Beyazıt, Nevrin Altınkum, Sina Yılankaya, Şevket Tunç and Ürün Eşen for their friendship.

Last but not least, I would like to thank my family Pınar Ersoy, Levent Ersoy, Tanju Ersoy and especially my mom Fatma Ersoy who have supported me and been there for me through my life. And I would like to thank Lotus for being our cat.

ABSTRACT

DESIGN OF DONOR-ACCEPTOR CONJUGATED POLYMERS FOR HIGH-PERFORMANCE ORGANIC SOLAR CELLS: A QUANTUM MECHANICAL APPROACH

In this study, the design of donor-acceptor conjugated polymers for high-performance organic solar cells is intended by investigating electronic, geometrical and optical properties of a specific set of donors that are used in polymer solar cells. 4 different donors including benzo [1,2-b:4,5-b'] dithiophene (BDT), 3,3'-difluoro-2,2'-bithiophene (diF2T), naphtho [1,2-b:5,6-b'] dithiophene (NDT), thieno[3,2-b] thiophene (TT) and 1 acceptor named 2-propyl-5,6-difluorobenzo[d][1,2,3]triazole(ffTAZ) are studied in order to set a benchmark. The 4 different donors studied for benchmarking and 7 different acceptors including benzo [c] [1,2,5] thiadiazole(cop1), [1,2,5] thiadiazolo [3,4-g] quinoxaline (cop2), [1,2,5] thiadiazolo [3,4-d] pyri-dazine (cop3), [1,2,5] thiadiazolo [3,4-c] pyridine (cop4), [1,2,5] oxadiazolo [3,4-d] pyri-dazine (cop5), fluorinated naphtho [1,2-c:5,6-c'] bis [1,2,5] thiadiazole (FNTz), fluori-nated [2,1,3] benzobisthiadiazole (FBTz) are combined and investigated for 28 different predictions. Geometrical and optical characteristics were calculated using Density Functional Theory (DFT). Distortion energies and reorganizational energies for electron and hole transfer were calculated using B3LYP/6-311G*.

In conclusion, 2 out of 28 molecules were chosen as the most effective molecules to be used in high-performance organic solar cells. The molecules chosen contain NDT and TT as donors and FBTz as acceptor.

ÖZET

YÜKSEK PERFORMANSLI ORGANİK GÜNEŞ PİLLERİ İÇİN KONJUGE POLİMERLERİN TASARIMININ KUANTUM MEKANİĞİ İLE İNCELENMESİ

Bu çalışmada, yüksek performanslı organik güneş pillerindeki konjuge polimerlerin tasarımı için polimer güneş pillerinde bulunan belirli bir grup vericinin elektronik, optik ve geometrik özellikleri incelenmiştir. Referans noktası belirlemek için kullanılan 4 farklı vericinin isimleri benzo [1,2-b:4,5-b'] dithiophene (BDT), 3,3'-difluoro-2,2'-bithiophene (diF2T), naphtho [1,2-b:5,6-b'] dithiophene (NDT), thieno[3,2-b] thiophene (TT) iken 1 alıcının ismi de 2-propyl-5,6-difluorobenzo[d][1,2,3]triazole(ffTAZ)'dir. İsimleri benzo [c] [1,2,5] thiadiazole(cop1), [1,2,5] thiadiazolo [3,4-g] quinoxaline (cop2), [1,2,5] thiadiazolo [3,4-d] pyri-dazine (cop3), [1,2,5] thiadiazolo [3,4-c] pyridine (cop4), [1,2,5] oxadiazolo [3,4-d] pyri-dazine (cop5), fluorinated naphtho [1,2-c:5,6-c'] bis [1,2,5] thiadiazole (FNTz) ve fluori-nated [2,1,3] benzobisthiadiazole (FBTz) olan 7 farklı alıcı birleştirilmiş ve toplamda 28 molekül incelenmiştir. Moleküllerin geometrik ve optik özellikleri yoğunluk fonksiyonel teorisi (DFT) kullanılarak; bükülme ve reorganizasyon enerjileri ise B3LYP/6-311G* ile hesaplanmıştır.

Sonuç olarak, incelenen 28 farklı molekülden 2 tanesi yüksek performanslı güneş pilleri için en verimli moleküller olarak seçilmiştir. Seçilen iki molekül verici olarak NDT ve TT alıcı olarak da FBTz'den oluşmaktadır.

TABLE OF CONTENTS

ACKNOWLEDGEMENTS iii
ABSTRACT iv
ÖZET v
LIST OF FIGURES viii
LIST OF TABLES xii
LIST OF SYMBOLS xv
LIST OF ACRONYMS/ABBREVIATIONS xvii
1. INTRODUCTION 1
2. AIM OF THE STUDY 11
3. METHODOLOGY 12
3.1. Density Functional Theory 12
3.2. Basis Sets 17
3.3. Time Dependent Density Functional Theory 18
3.4. Conformer Search 20
3.5. Geometries 20
3.6. Distortion Energies 20
3.7. Reorganization Energies 21
3.8. Natural Transition Orbitals 23
4. RESULTS 26
4.1. Benchmark Calculations 26
4.1.1. Geometries 29
4.1.2. Choice of Methodology 36
4.1.3. HOMO, LUMO and E_g Values 42
4.1.4. Distortion Energies 43
4.1.5. Reorganization Energies 44
4.1.6. Natural Transition Orbitals 45
4.2. Molecules Under Investigation 50
4.2.1. Geometries 50
4.2.2. HOMO, LUMO and E_g Values 50

4.2.3. Distortion Energies 61
4.2.4. Reorganization Energies 61
4.2.5. Selection of Suitable Molecules 61
5. CONCLUSION 67
REFERENCES 68

LIST OF FIGURES

Figure 1.1. Global Energy Consumption in Fraction, 2017 1

Figure 1.2. Basic design of the four CSP types: (A) Solar Power Tower, (B) Parabolic Trough, (C) Linear Fresnel Reflector, (D) Parabolic Dish. [1] 4

Figure 1.3. Structures of Single-Layer and Multi-Layer Photovoltaic Solar Cells 8

Figure 1.4. Structure of A Bulk Hetero-Junction (BHJ) Solar Cell [2] 8

Figure 1.5. Fundamental Steps of Charge Transfer Occurring in Donor-Acceptor BHJ Solar Cells 9

Figure 3.1. Internal reorganization energy $\lambda_+ + \lambda_0$ for Hole Transfer, and Adiabatic Ionization Energy, ΔE 22

Figure 3.2. Internal reorganization energy $\lambda_- + \lambda_0$ for Electron Transfer, and the Adiabatic Ionization Energy, ΔE 22

Figure 4.1. Structures of Donors: (a) BDT (b) diF2T (c) NDT (d) TT 27

Figure 4.2. Structures of Benchmark Molecules: (a) P-BDT (b) P-diF2T (c) P-NDT (d) P-TT 27

Figure 4.3. Representation of five different states: (a) Neutral Ground State (b) Oxidized Doublet State (c) Singly Reduced Doublet State (d) Neutral Triplet State (e) TD-DFT State [3] 28

Figure 4.4. Geometry of P- Polymer 30

Figure 4.5. All Possible Conformations of P- Polymer: (a) dddd (b) dddu (c) ddud (d) dduu (e) dudd (f) duud (g) duuu (h) uddd (i) uddu (j) uduu (k) uudd (l) uudu (m) uuud (n) uuuu (B3LYP/6-311G*) . . 31

Figure 4.6. All Possible Conformations of P-BDT: (a) dd (b) du (c) ud (d) uu 32

Figure 4.7. All Possible Conformations of P-diF2T: (a) dd (b) du (c) ud (d) uu 33

Figure 4.8. All Possible Conformations of P-NDT: (a) dd (b) du (c) ud (d) uu 34

Figure 4.9. All Possible Conformations of P-TT: (a) dd (b) du (c) ud (d) uu . 35

Figure 4.10. Dihedral Angles of Benchmark Molecules 43

Figure 4.11. Natural Transition Orbitals of P-BDT, B3LYP/6-311G* 46

Figure 4.12. Natural Transition Orbitals of P-diF2T, B3LYP/6-311G* 47

Figure 4.13. Natural Transition Orbitals of P-NDT, B3LYP/6-311G* 48

Figure 4.14. Natural Transition Orbitals of P-TT, B3LYP/6-311G* 49

Figure 4.15. Structures of Acceptors: (a) cop1 (b) cop2 (c) cop3 (d) cop4 (e) cop5 (f) FBTz (g) FNTz 51

Figure 4.16. Structures of Molecules with cop1 as the Acceptor Unit: (a) cop1-BDT (b) cop1-diF2T (c) cop1-NDT (d) cop1-TT 52

Figure 4.17. Structures of Molecules with cop2 as the Acceptor Unit: (a) cop2-BDT (b) cop2-diF2T (c) cop2-NDT (d) cop2-TT 52

Figure 4.18. Structures of Molecules with cop3 as the Acceptor Unit: (a) cop3-BDT (b) cop3-diF2T (c) cop3-NDT (d) cop3-TT 53

Figure 4.19. Structures of Molecules with cop4 as the Acceptor Unit: (a) cop4-BDT (b) cop4-diF2T (c) cop4-NDT (d) cop4-TT 53

Figure 4.20. Structures of Molecules with cop5 as the Acceptor Unit: (a) cop5-BDT (b) cop5-diF2T (c) cop5-NDT (d) cop5-TT 54

Figure 4.21. Structures of Molecules with FBTz as the Acceptor Unit: (a) FBTz-BDT (b) FBTz-diF2T (c) FBTz-NDT (d) FBTz-TT 54

Figure 4.22. Structures of Molecules with FNTz as the Acceptor Unit: (a) FNTz-BDT (b) FNTz-diF2T (c) FNTz-NDT (d) FNTz-TT 55

Figure 4.23. 3D Structures of (a) cop1-BDT (b) cop1-diF2T (c) cop1-NDT (d) cop1-TT 55

Figure 4.24. 3D Structures of (a) cop2-BDT (b) cop2-diF2T (c) cop2-NDT (d) cop2-TT 56

Figure 4.25. 3D Structures of (a) cop3-BDT (b) cop3-diF2T (c) cop3-NDT (d) cop3-TT 56

Figure 4.26. 3D Structures of (a) cop4-BDT (b) cop4-diF2T (c) cop4-NDT (d) cop4-TT 57

Figure 4.27. 3D Structures of (a) cop5-BDT (b) cop5-diF2T (c) cop5-NDT (d) cop5-TT 57

Figure 4.28. 3D Structures of (a) FBTz-BDT (b) FBTz-diF2T (c) FBTz-NDT (d) FBTz-TT 58

Figure 4.29. 3D Structures of (a) FNTz-BDT (b) FNTz-diF2T (c) FNTz-NDT (d) FNTz-TT 58

Figure 4.30. Natural Transition Orbitals of FBTz-NDT, B3LYP/6-311G* . . . 65

Figure 4.31. Natural Transition Orbitals of FBTz-TT, B3LYP/6-311G* 66

LIST OF TABLES

Table 4.1. Experimental HOMO, LUMO and E_g (eV) Values of P-BDT, P-diF2T, P-NDT and P-TT 29

Table 4.2. Electronic Energies (Hartree), Relative Electronic Energies (kcal/mol) and Total Dipole Moment of the Conformations of P- Polymer, B3LYP/6-311G* 30

Table 4.3. Electronic Energies (Hartree), Relative Electronic Energies (kcal/mol) and Total Dipole Moment of the Conformations of P-BDT, B3LYP/6-311G* 32

Table 4.4. Electronic Energies (Hartree), Relative Electronic Energies (kcal/mol) and Total Dipole Moment of the Conformations of P-diF2T, B3LYP/6-311G* 33

Table 4.5. Electronic Energies (Hartree), Relative Electronic Energies (kcal/mol) and Total Dipole Moment of the Conformations of P-NDT, B3LYP/6-311G* 34

Table 4.6. Electronic Energies (Hartree), Relative Electronic Energies (kcal/mol) and Total Dipole Moment of the Conformations of P-NDT, B3LYP/6-311G* 35

Table 4.7. Five States of P-BDT Molecule (B3LYP/6-311G*), (ωB97XD/6-311G*), (PBE0/6-311G*), (M06-2X/6-311G*) and Their Absolute Percentage Errors From Experimental Values (eV) 38

Table 4.8. Five States of P-diF2T Molecule (B3LYP/6-311G*), (ωB97XD/6-311G*), (PBE0/6-311G*), (M06-2X/6-311G*) and Their Absolute Percentage Errors From Experimental Values (eV) 39

Table 4.9. Five States of P-NDT Molecule (B3LYP/6-311G*), (ωB97XD/6-311G*), (PBE0/6-311G*), (M06-2X/6-311G*) and Their Absolute Percentage Errors From Experimental Values (eV) 40

Table 4.10. Five States of P-TT Molecule (B3LYP/6-311G*), (ωB97XD/6-311G*), (PBE0/6-311G*), (M06-2X/6-311G*) and Their Absolute Percentage Errors From Experimental Values (eV) 41

Table 4.11. HOMO, LUMO and E_g Values of P-BDT, P-diF2T, P-NDT and P-TT for Neutral Ground State in B3LYP/6-311G* 42

Table 4.12. HOMO, LUMO and E_g Values of P-BDT, P-diF2T, P-NDT and P-TT for Reduced State in PBE0/6-311G* 43

Table 4.13. Dihedral Angles and Total Distortion Energies in kcal/mol for P-BDT, P-diF2T, P-NDT and P-TT Molecules 44

Table 4.14. Reorganization Energies in meV and AIP, AEA, VIP and VEA values in eV for P-BDT, P-diF2T, P-NDT and P-TT 44

Table 4.15. HOMO, LUMO and E_g Values for Molecules Under Investigation, Neutral Ground State (B3LYP/6-311G*) (eV) 59

Table 4.16. HOMO, LUMO and E_g Values for Molecules Under Investigation, Reduced State (PBE0/6-311G*) (eV) 60

Table 4.17. Dihedral Angles and Distortion Energies in kcal/mol of Studied Molecules 62

Table 4.18. Reorganization Energies for Hole and Electron and AIP, AEA, VIP and VEA Values for Studied Molecules 63

LIST OF SYMBOLS

$E_{xc}[\rho]$	The exchange-correlation functional energy
$E_x[\rho]$	Exchange functional
$E_c[\rho]$	Correlation functional
h_i	One-electron Hamiltonian
$\hbar$	Planck's constant divided by 2π
$\hat{H}$	Hamiltonian Operator
J_{SC}	Short Circuit Current
$J[\rho]$	Coulomb energy
m_e	The mass of electron
m_k	The mass of nucleus
r_{ij}	The distance between the particles
$T(\rho)$	The kinetic energy of the interacting electrons
$T_s(\rho)$	The kinetic energy of non-interacting electrons
$\hat{T}(\underline{r})$	The kinetic energy of electrons
$V_{ee}[\rho]$	The electronic interaction energy
$\hat{V}_{ext}(\underline{r}, t)$	The time-dependent potential
V_{OC}	Open Circuit Voltage
$\hat{W}(\underline{r})$	The Coulomb interaction between the electrons
Z	Atomic number
ΔG_{cs}	Thermodynamic Driving Force of Charge Split
$\lambda_{electron}$	Reorganization Energy For Electrons
λ_{hole}	Reorganization Energy For Holes
$\rho(x)$	Electron Density
ψ	Eigenfunction
ψ_{HP}	Hartree Product wavefunction
Ψ_i	Occupied Spin Orbitals
Ψ'_a	Unoccupied Spin Orbitals

∇^2	The Laplacian operator

LIST OF ACRONYMS/ABBREVIATIONS

AC	Alternative Current
B	Becke's 1988 Functional
B3LYP	Becke-3-parameter Lee-Yang-Parr Functional
B88	Becke 88 Exchange Functional
BHJ	Bulk Hetero-Junction
BRx	The 1989 Exchange Functional of Becke
CdTe	Cadmium Telluride
CIGS	Copper Indium Gallium Selenide
CIS	Configuration Interaction Singles
CSP	Concentrated Solar Power
DC	Direct Current
DFT	Density Functional Theory
DSSCs	Dye-sensitized Solar Cells
FF	Fill Factor
G96	The 96 Exchange Functional of Gill
GTO	Gaussian Type Orbital
HOMO	Highest Occupied Molecular Orbital
ITO	Tin Doped Indium Oxide
LC	Long-Rage Corrected
LDA	Local Density Approximation
LUMO	Lowest Unoccupied Molecular Orbital
LFR	Linear Fresnel Reflector
LYP	Correlation Functional of Lee Yang Parr
M06-2X	Empirical Exchange Correlation Functional
mPW	The Perdew-Wang 1991 Functional
NTO	Natural Transition Orbital
O	Handy's OPTX modification of Becke's Exchange Functional
PBE	The 1996 Functional of Perdew-Burke-Ernzerhof

PBE0	The Hybrid Functional of Perdew-Bucke-Ernzerhof
PBEh	The 1998 Revision of PBE
PCE	Power Conversion Efficiency
PKZB	The Exchange Part of The Perdew-Kurth-Zupan-Blaha Functional
PL	Perdew's Local Functional
PV	Photovoltaics
PW91	The Exchange Component of Perdew and Wang's 1991 Functional
revTPSS	The Revised TPSS Exchange Functional of Perdew et. al.
S	Slater Exchange or Local Spin Density Exchange Functional
SCF	Self-Consistent Field
SPT	Solar Power Tower
TD-DFT	Time Dependent Density Functional Theory
TPSS	The Exchange Functional of Tao-Perdew-Staroverow-Scuseria
TW	Terawatts
VWN	The 1980 Correlation Functional of Vosko-Wilk-Nusair
VWN5	Functional V
wPEh	The Exchange Part of Screened Coulomb Potential-Based Final of Heyd-Scuseria-Ernzerhof
XA	XAlpha Exchange Functional
ωB97XD	Head-Gordon and Coworkers Hybrid Density Functional

1. INTRODUCTION

One of the most controversial issues in today's world is how energy sources have been produced as the worldwide consumption of energy has grown significantly and energy supplies need to be on desired levels in order to meet this requirement.

Three main types of energy sources are fossil fuels including natural gas, oil and coal, nuclear energy and clean energy including solar, wind, water, geothermal and biomass energy. Carbon based fossil energy sources, consisting of oil, coal and natural gas, were formed from buried organic materials including dead plants and animals. Nuclear energy source is provided by nuclear fission, the combination of two small atoms into a larger one, or nuclear fusion, the split of a large atom into smaller ones, in order to generate electricity and evaporate water. In 2017, global energy consumption rate of carbon based fossil fuels and nuclear energy was recorded as 89.60% [4] meaning that carbon based fossil fuels along with nuclear energy are the main energy source for the world.

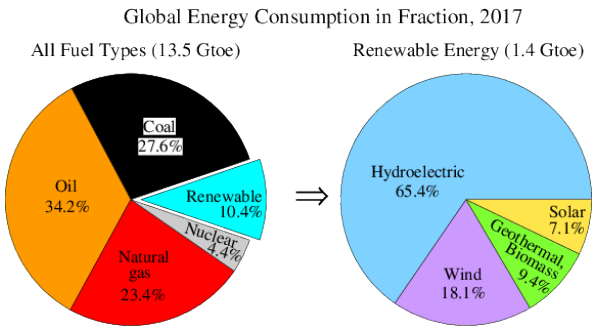

Figure 1.1. Global Energy Consumption in Fraction, 2017

The reasons of preferring carbon based fossil fuels as the primary energy source are their being a cheap source of energy, they're safe to transport, they have massive economic benefits, they're completely stable because of containing carbon and hydrogen molecules, they have high calorific values which means they're more effective as energy

sources, they're abundant meaning they're found almost in every country in the world, they have useful byproducts (plastics for instance), they're more reliable compared to renewable energy sources, they create numerous jobs in the fields of construction, finance and administration, they're easier to extract and process and are capable to generate massive amount of energy at a single location.

On the other hand, carbon based fossil fuels have severe adverse environmental effects. The primary negative effect is their contribution to global warming and greenhouse effect through carbon dioxide emission. Negative effects of carbon dioxide emissions are shrinking water supplies as carbon dioxide persists in the atmosphere from 50 to 200 years, increasing incidents of severe weather including wildfires, droughts and tropical storms, changes in food supply as agricultural industry and the human food supply are affected through changing weather. Geographical changes as small changes in temperature have substantial effects on geographical features. The other negative outcomes of carbon based fossil fuels are their being non-renewable energy sources meaning the amount of reserves available is finite, release of sulfur dioxide from coal and oil causing breathing problems for living creatures and contributing to acid rain and government income tax incentives that subsidize domestic production of fossil fuels.

Nuclear energy is the second most consumed energy source in the world. The reasons of choosing nuclear power are their emitting relatively low amounts of carbon dioxide compared to fossil fuels, their being readily available sources and their capability of generating massive amount of electrical energy in a single plant. However, as carbon based fossil fuels, nuclear power energy has several negative outcomes including the radioactive waste from nuclear plants which has caused the death of many living creatures, the possibility of radioactive wastes' turning into nuclear weapons and its being a rare resource as its main energy source is uranium which is estimated to last in a near future depending on the actual demand.

The common issue about fossil fuels and nuclear energy is that both of them are non-renewable energy sources meaning their sources are limited and they will not

last forever. In addition to this, the environmental effects of consuming carbon based fossil fuels or nuclear energy have been discussed in several studies, and in order to eliminate these problems and provide a sustainable future, finding alternative and renewable energy sources have become the focus of researchers. The environmental sustainability concept can be described as a condition of equilibrium, resilience and interconnection that enables people to satisfy their needs while not surpassing the ability of its supporting ecosystems to continue to regenerate the services needed to meet those needs or by our actions that diminish biological diversity. In order to meet the conditions of sustainability, discovery and efficiency improvements of energy productions through renewable energy sources have become a substantial issue.

The five primary types of renewable energy are solar, water, wind, geothermal and biomass energy including bio-energy crops, agricultural residue, municipal waste organic component, industrial waste and forestry residue. Each type has its own disadvantages in terms of the environmental cost, abundance and sustainability. Disadvantages of geothermal energy are that deep geothermal energy is expensive to utilize, during the exploitation process harmful gasses may be released into atmosphere and the exploitation process may cause earthquakes. Biomass energy suffers from the following disadvantages; biomass is not available for large-scale production, the production of biomass energy is expensive, the space for food production becomes less as land is used for biomass production, over-cultivation may lead to destruction of water supply and biomass power plants may release greenhouse gasses into atmosphere. The drawbacks of water energy so-called hydro-power are the construction of a hydro-power station which is expensive, building a reservoir dam which can alter the ecosystem & landscape and hydro-power stations which compete for a location with other uses of land like agricultural issues. Wind energy has the following disadvantages; the construction of wind turbines are expensive, the contact with turbines kills birds and turbines only work in windy locations.

Taking into account the disadvantages of other renewable energy sources, it can be safely stated that solar energy is the most convenient renewable energy source. More energy from the sun light strikes the earth in one hour than all of the energy consumed

by humans in an entire year [1]. With approximately 89,000 terawatts (TW) of energy potential, solar energy has the greatest theoretical potential of renewable energy [5]. Approximately, 13 TW of energy is required in order to sustain the lifestyle of all individuals on earth and an additional 10 TW are required in order to maintain the current lifestyle [6]. Hence, cost and efficiency of solar cells should be improved in order to be consumed as primary energy source.

Two primary technologies by which solar energy is exploited are concentrated solar power (CSP) systems and photovoltaic (PV) systems.

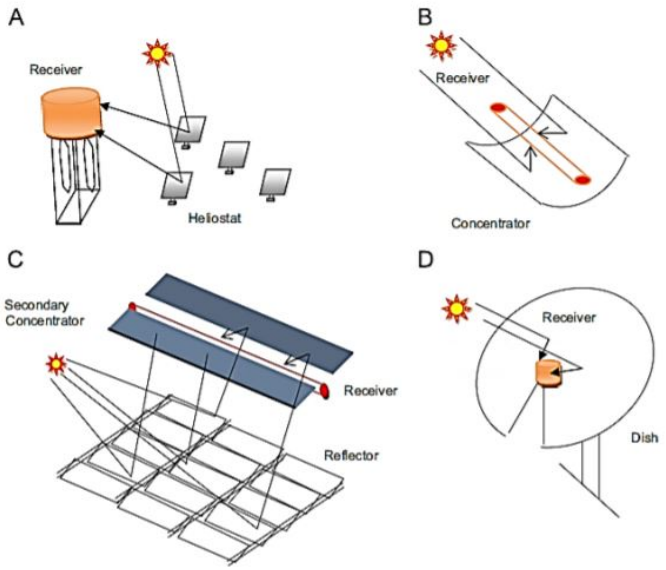

Figure 1.2. Basic design of the four CSP types: (A) Solar Power Tower, (B) Parabolic Trough, (C) Linear Fresnel Reflector, (D) Parabolic Dish. [1]

Concentrated solar power or concentrating solar power or concentrated solar thermal technologies (CSP) use separate mirrors in order to focus the sun's energy onto a single point where it is collected and converted into heat or thermal energy which can be used to generate electrical power. Four members of CSP family are solar power tower (SPT) or central receiver systems, parabolic trough systems, linear Fresnel reflector (LFR) and parabolic dish systems. In solar power tower (SPT) systems, a tower is placed in the center of a large array of mirrors in order to convert energy from the sun

into electrical power. Parabolic trough systems use parabola-shaped reflectors covered with mirror in order to concentrate sunlight onto a liquid filled tube. Linear Fresnel reflector (LFR) systems catch the sun's energy with large mirrors in order to focus and reflect the sunlight onto a heated fluid container tube. Parabolic dish systems use a parabolic dish of mirrors in order to direct and concentrate sunlight onto a receiver mounted at the focal point which produces electricity. CSP systems have the ability to store energy in order to generate electrical power. Unlikely, PV systems cannot store or produce thermal energy as they directly produce electrical energy. But when it comes to consider the three primary factors in deciding on energy sources which are cost of energy, accompanying services and power dispatch ability on demand, it can be safely stated that PV systems remain a preferable solution over CSP systems.

PV systems composed of one or more solar panels, which are solar cells or PV cells wired in series, combined with an inverter and other semi-conducting materials which use sunlight in order to generate electrical current directly. Photons, the light from the sun in packets of energy, fall onto a solar panel and cause photovoltaic effect which is a process in which two dissimilar materials in close contact produce an electrical voltage when struck by light or other radiant energy. The electrical voltage is in direct current (DC) form which can be converted to alternative current (AC) form with the help of the inventer used. Solar cell types can be classified as amorphous silicon solar cells (a-Si), bio-hybrid solar cells, cadmium telluride solar cells (CdTe), concentrated PV cells (CVP and HCVP), copper indium gallium selenide solar cells (CI(G)S), crystalline silicon solar cells (c-Si), dye-sensitized solar cells (DSSC), gallium arsenide germanium solar cells (GaAs), hybrid solar cell, luminescent solar concentrator cells (LSC), micromorph (tandem-cell using a-Si/μc-Si), monocrystalline solar cells (mono-Si), multi-junction solar cells (MJ), nanocrystal solar cells, organic solar cells (OPV), perovskite solar cells, photoelectrochemical cells (PEC), plasmonic solar cells, polycrystalline solar cells (multi-Si), quantum dot solar cells, solid-state solar cells, thin-film solar cells (TFSC), wafer solar cells, or wafer-based solar cell crystalline and non-concentrated heterogeneous PV cells.

The most common type of solar cells are inorganic solar cells as their efficiency is higher than the other types. Si, CdTe and CIGS (copper indium gallium diselenide) can be listed as the most widely used inorganic solar cell materials [7].

Two types of silicon based solar cells are n-type and p-type respectively. The p-type silicon based solar cells are generated through adding atoms like boron or gallium. An electron hole is created as for bond formation, the number of valence electrons in boron atom is one less than the number of those in silicon atom. The n-type silicon based solar cells on the other hand, are formed through adding a phosphorus atom whose number of valence electrons is one more than that of silicon atom resulting in an unpaired electron to move freely. Since p-type has higher resistance to space radiation than n-type, the former one is more producible and accessible nowadays although the latter one has been produced since 1950's. However, n-type crystalline Si solar cells have higher efficiency by about 20-25% [8]. The most significant disadvantage of this type is the need of high purity and high fabrication cost.

CdTe based solar cells are generated through the thin film of CdTe which is utilized for absorbing sunlight and converting it to electricity. Although CdTe solar cells' efficiency is about 13.6%, they are not as efficient as Si solar cells. As CdTe solar cells are flexible in the surface layer, they have an important supremacy in having higher power/mass ratio [9]. The drawbacks of CdTe solar cells are that Cd is a toxic substance and Te is not an abundant atom.

CIGS based solar cells are obtained from a substrate like glass, a back contact like Mo, an absorber layer like Cu $(In_{1-x}, Ga_x)\ Se_2$, buffer layers like CdS, InS, ZnS, ZnO and ZnSe, a window layer like i-ZnO and a TCO layer like n-ZnO:Al. Advantages of CIGS thin film solar cells are high absorption of sunlight, band gap of absorber layer which is easy to control and has long term stability. The efficiency of CIGS with CdS buffer layer is about 19%, meaning their efficiency is higher than CdTe solar cells. As an absorber layer, cadmium is a toxic substance [10]. CIGS solar cells' both efficiency and abundance are not as high as those of CdTe solar cells. Another negative outcome of CIGS solar cells is their high production cost.

Dye-sensitized solar cells (DSSCs) consist of three parts which can be listed as a dye-sensitized TiO_2 photoanode, an iodide/triiodide redox electrolyte and a counter electrode [11]. Photoactive dye becomes active and excites electrons by catching photons when exposed to sunlight. Excited electrons are sent to a TiO_2 semiconductor which helps electrons been transmitted to external circuit connected to the DSSC. Electrons come back to the dye with the redox reactions via an iodide/triiodide redox electrolyte. Advantages of DSSCs are their being low cost materials, their having simple fabrication processes and high conversion efficiency [11].

Perovskite solar cells' general chemical formula is ABX_3, where A is an organic cation, B is a divalent metal ion and X is a halide or any other combination. Power conversion efficiency of perovskite solar cells has been calculated to be greater than 20% recently. One of their major drawbacks is that they are degradable when exposed to moisture and oxygen. Beside their advantages like being easy to fabricate and capable of strong absorption, lead is a highly toxic substance hence, perovskite solar cells should not be utilized in terms of actions related to human health [12]

Inorganic semiconductors with their band gap energies give better matching to solar spectrum whereas organic semiconductors have higher absorptivities, lower cost and 2000 times thinner layers than inorganic materials [13]. Organic solar cells are composed of carbon based molecules which convert sunlight to electric energy. The advantages of organic solar cells include low cost, light weight, long life time and the soluble capability to produce flexible large-area devices [14].

In the literature, primary types of organic photovoltaic solar cells are single-layer organic solar cells, multi-layer organic solar cells and bulk hetero-junction (BHJ) solar cell devices [15]. Single-layer organic solar cells are generated through inserting organic electronic substances like a small molecule and polymer between two electrodes. Multi-layer organic cells are generated and an electron rich donor and an electron deficient acceptor are put together between two electrodes. Figure 1.3. demonstrates their structure.

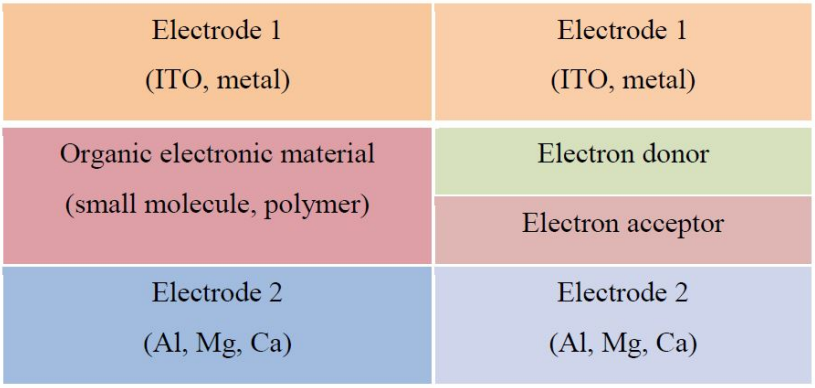

Figure 1.3. Structures of Single-Layer and Multi-Layer Photovoltaic Solar Cells

BHJ solar cells are preferred because of low cost, light weight and fast/cheap roll-to-roll production. In a BHJ solar cell, the active layer is placed between a transparent anode, typically tin doped indium oxide (ITO), and a metal cathode. A thin layer of poly(3,4-ethylenedioxythiophene) - poly(styrenesulfonate) (PEDOT:PSS) is inserted between the ITO and the active layer in order to raise the electrical contact and calibrate energy levels. The active layer is made up of two components such as any electron donor as the conjugated polymer and any electron acceptor that generally is used as fullerene derivatives. Figure 1.4 demonstrates the structure of a BHJ solar cell [2].

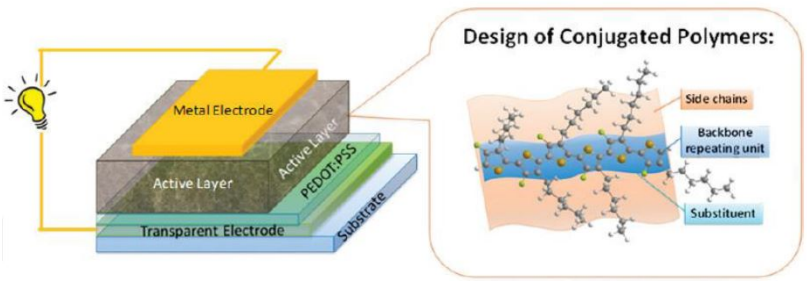

Figure 1.4. Structure of A Bulk Hetero-Junction (BHJ) Solar Cell [2]

Organic semiconductors are organic substances that have the capability of transferring charge carriers. A standard organic solar cell contains an active layer with

a p-type semiconductor as the donor, and an n-type semiconductor as the acceptor. Charge carriers are holes and electrons in p orbitals of the semiconductor, and the charge transfer is subject to the movement of these carriers from one molecule to the other. The energy difference between the highest occupied molecular orbital (HOMO) level and the lowest unoccupied molecular orbital (LUMO) level influences the charge motion rate and efficiency. It is feasible to arrange the physical characteristics of an organic semiconductor material: HOMO/LUMO levels, charge carrier mobility and crystal structure can be adjusted by chemical modifications [16]. Merging correct donor and acceptor groups bearing these requirements in mind will let us have the optimized device structure.

Figure 1.5. shows the charge transfer mechanism in donor-acceptor bulk hetero-junction solar cells.

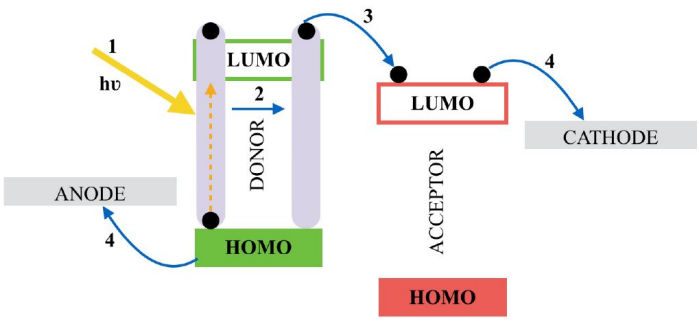

Figure 1.5. Fundamental Steps of Charge Transfer Occurring in Donor-Acceptor BHJ Solar Cells

The first step of the mechanism is the donors' generation of excitons instead of electrons. In the second step, in order to separate, the excitons diffuse into donor-acceptor interface and unless they are able to reach the interface, they recombine. In the third step of the mechanism, separation occurs in order to transfer an electron into the acceptor layer. In the final step, the charge is accumulated at the external electrodes.

The definition of Power Conversion Efficiency (PCE) is the measure of incoming light converted to electricity. The PCE can be maximized by maximizing the short circuit current (J_{SC}) density , the fill factor (FF), and the open circuit voltage (V_{OC}). Short circuit current density is associated with charge carrier density and the charge carrier mobility. Raising these two parameters will produce an increase in J_{SC}. Short circuit current density is also maximized by reducing the electronic excitation energy of the donor, which will cause a rise in the thermodynamic driving force of charge split (ΔG_{cs}) at the donor-acceptor interface. Open circuit voltage (V_{OC}) is associated with the highest occupied molecular orbital (HOMO) level of the donor and lowest unoccupied molecular orbital LUMO level of the acceptor [17,18]. Open circuit voltage is also influenced by the nano-morphology of the active layer in the polymer fullerene bulk hetero-junction solar cells [19]. V_{OC} is maximized by raising the LUMO energy of the acceptor and reducing the HOMO energy of the donor. However, as reducing the HOMO of the donor raises the energy difference, maximization of J_{SC} and V_{OC} must be balanced. Fill factor is altered by charge carriers reaching the electrodes [20], and is influenced by charge split, mobility and the morphological characteristics of the device, like active layer depth.

2. AIM OF THE STUDY

In this study, the design of donor-acceptor conjugated polymers for high - performance organic solar cells is analyzed by investigating electronic, geometrical and optical properties of a specific set of donors that are used in non-fullerene polymer solar cells. 4 different donors [21] including benzo [1,2-b:4,5-b'] dithiophene (BDT), 3,3'-difluoro-2,2'-bithiophene (diF2T), naphtho [1,2-b:5,6-b'] dithiophene (NDT), thieno [3,2-b] thiophene (TT) and 1 acceptor named 2-propyl-5,6-difluorobenzo[d][1,2,3]triazole (ffTAZ) are studied in order to set a benchmark. The 4 different donors studied for benchmarking and 7 different acceptors [22,23] including benzo [c] [1,2,5] thiadiazole (cop1), [1,2,5] thiadiazolo [3,4-g] quinoxaline (cop2), [1,2,5] thiadiazolo [3,4-d] pyridazine (cop3), [1,2,5] thiadiazolo [3,4-c] pyridine (cop4), [1,2,5] oxadiazolo [3,4-d] pyridazine (cop5), fluorinated naphtho [1,2-c:5,6-c'] bis [1,2,5] thiadiazole (FNTz), fluorinated [2,1,3] benzobisthiadiazole (FBTz) are combined and investigated for 28 different species. In total, 32 molecules will be investigated.

Basically, this study aims to come up with an appropriate computational approach in order to find the eligible donor-acceptor pairs for high-performance organic solar cells.

3. METHODOLOGY

The goal of this chapter is to express the theoretical background of the density functional theory, basis sets, properties of the functionals and basis sets used for the calculations, time-dependent density functional theory, conformer search, geometry optimizations, natural transition orbitals, distortion and reorganization energies. Quantum chemical calculations are performed using Gaussian '09 [24] software.

3.1. Density Functional Theory

Density functional theory (DFT) is a computational quantum mechanical approach. [25] To put it in other words, Schrödinger's equation which helps finding the wavefunction of the system, cannot be solved for many-body systems. Density functional theory gives an opportunity to obtain an approximate solution to the Schrödinger's equation and determine the wavefunction for many-body systems. In quantum mechanics, the exact position and the momentum of a particle cannot be measured at the same time. So, the position is demonstrated as the probability, which is the square of the wavefunction, of finding that particle in a given space.

$$H\psi = E\psi \tag{3.1}$$

where H is Hamiltonian that expresses the system energy as an eigenvalue.

$$-\sum_i \frac{\hbar^2}{2m_e}\nabla_i^2 - \sum_k \frac{\hbar^2}{2m_k}\nabla_k^2 - \sum_i \sum_k \frac{e^2 Z_k}{r_{ik}} + \sum_{i<j} \frac{e^2}{r_{ij}} + \sum_{k<l} \frac{e^2 Z_k Z_l}{r_{kl}} \tag{3.2}$$

where i and j are electrons, k and l are nuclei, $\hbar$ is Planck's constant divided by 2π, m_k is the mass of nucleus, m_e is the mass of electron, ∇^2 is the Laplacian operator, Z is atomic number and r_{ij} is the distance between the particles.

In Equation 3.2, it can be stated that five different parameters, which are the motion of the electrons, the motion of the nuclei, the attraction of electrons to the nuclei, the interelectronic repulsions and the internuclear repulsions respectively, affect the energy of a system.

Equation 3.1. might have an infinite set of solutions consisting of different eigenfunctions ψ each of which is associated to an eigenvalue E, meaning for each eigenfunction ψ_i, there exists an eigenvalue E_i.

$$H\psi_n = E\psi_n(x), n = 1, 2, 3, ... \tag{3.3}$$

Since the electron-electron interaction term in the original Hamiltonian derived for the system is too complicated, it is extremely hard to determine the accurate solution of the Schrödinger's equation for many-body systems. Therefore, in order to determine an approximate solution, the wavefunction defining the whole system should be splitted to the product of many one-electron systems such as $\chi_1(1)$, $\chi_2(2)$, $\chi_3(3)$,... When Hamiltonian is made up of one-electron kinetic energy and nuclear attraction terms, it can be splitted:

$$H = \sum_{i=1}^{N} h_i \tag{3.4}$$

where h_i is one-electron Hamiltonian and N is the number of electrons.

$$h_i = -\frac{1}{2}\nabla_i^2 - \sum_{k=1}^{M} \frac{Z_k}{r_{ik}} \tag{3.5}$$

where M shows the total number of nuclei.

Therefore, the equation below should be solved:

$$h_i\psi_i = \varepsilon_i\psi_i \tag{3.6}$$

for eigenvalues of one-electron Hamiltonian in the the one-electron Schrödinger's equation. As the Hamiltonian operator described by Equation 3.4. is separable, its eigenfunctions can also be separated as;

$$\psi_{HP} = \psi_1\psi_2...\psi_N \tag{3.7}$$

where ψ_{HP} is Hartree Product wavefunction in which correction terms should be included since some of the interactions in the system are ignored.

In 1965, Kohn and Sham [26] realized that if the Hamiltonian is described for a non-interacting systems of electrons, calculations would not be that complicated.

The electron density $\rho(x)$ is:

$$\rho(x) = N \int ... \int \left|\Psi(x_1, x_2, ...x_n)\right|^2 dx_1 dx_2 ... dx_n \tag{3.8}$$

where both spins and spatial coordinates of electrons are demonstrated by x.

The electronic energy can be expressed as a function of the electron density:

$$E[\rho] = \int v(r)\rho(r)dr + T(\rho) + V_{ee}[\rho] \tag{3.9}$$

where $V_{ee}[\rho]$ is the electronic interaction energy and $T(\rho)$ is the kinetic energy of the interacting electrons. The electronic energy is defined as:

$$E[\rho] = \int v(r)\rho(r)dr + T_s(\rho) + J[\rho] + E_{xc}[\rho] \tag{3.10}$$

where $J[\rho]$ stands for coulomb energy, $T_s(\rho)$ is the kinetic energy of non-interacting electrons and $E_{xc}[\rho]$ is the exchange-correlation functional energy which is the sum of an exchange functional $E_x[\rho]$and a correlation functional $E_c[\rho]$

According to Kohn-Sham density functional theory [26]:

$$E[\rho(r)] = T_{ni}[\rho(r)] + V_{ne}[\rho(r)] + V_{ee}[\rho(r)] + \Delta T[\rho(r)] + \Delta V_{ee}[\rho(r)] \tag{3.11}$$

The exchange correlation energy E_{xc} includes both ΔT and ΔV_{ee} meaning the quantum mechanical exchange and the correlation, and the correction term for the classical self-interaction energy.

Local Density Approximation (LDA) is an approach in which a real non - homogeneous system is split into infinitesimal volumes whose electron density is taken as constant. The LDA approach cannot find the precise solution for the exchange energy which results in lack of observation of asymptotic behaviour of exchange energy density.

By combining the names for the correlation and exchange functionals, names for the different DFT models are given. In order to create a practicable approach, exchange functionals must be combined with a correlation functional resulting in the production of a hybrid functional.

Exchange functionals available in Gaussian are S (the Slater exchange also referred to as Local Spin Density exchange), XA (the XAlpha exchange), B (Becke's 1988 functional), PW91 (the exchange component of Perdew and Wang's 1991 functional), mPW (The Perdew-Wang 1991 functional), G96 (The 96 exchange functional of Gill), PBE (The 1996 functional of Perdew, Burke and Ernzerhof), O (Handy's OPTX modification of Becke's exchange functional), TPSS (the exchange functional of Tao, Perdew, Staroverow and Scuseria), RevTPSS (the revised TPSS exchange functional of Perdew et. al.), BRx (the 1989 exchange functional of Becke), PKZB (The exchange part of the Perdew, Kurth, Zupan and Blaha functional), wPBEh (the exchange part of screened Coulomb potential-based final of Heyd, Scuseria and Ernzerhof - also known as HSE) and PBEh (1998 revision of PBE).

Correlation functionals available in Gaussian are VWN (1980 correlation functional of Vosko, Wilk and Nusair), VWN5 (functional V which fits the Ceperly-Alder solution to the uniform electron gas), LYP (the correlation functional of Lee Yang and Parr), PL (Perdew Local - the 1981 non-gradient corrected functional of Perdew), P86 (the gradient corrections of Perdew, along with his 1981 local correlation functional), PW91 (Perdew and Wang's 1991 gradient-corrected correlation functional), B95 (Becke's τ-dependent gradient-corrected correlation functional), PBE (the 1996 gradient-corrected correlation functional of Perdew, Burke and Ernzerhof), TPSS (the τ-dependent gradient-corrected correlation functional of Tao, Perdew, Staroverov and Scuseria), RevTPSS (the revised TPSS correlation functional of Perdew et. al.), KCIS (the Krieger-Chen-Iafrate-Savin correlation functional), BRC (Becke-Roussel correlation functional) and PKZB (the correlation part of the Perdew, Kurth, Zupan and Blaha functional).

The four functionals used in this study are B3LYP, PBE0, ωB97XD and M06-2X.

B3LYP [27] which uses the non-local correlation provided by the LYP functional and VWN functional III for local correlation (not functional V) is the most widely used functional in quantum chemical calculations and it has the following form:

$$E_{xc} = E_{xc}^{LSDA} + a_1(E_x^{HF} - E_c^{LSDA}) + a_2\Delta E_x^{GC} + a_3\Delta E_c^{GC} \tag{3.12}$$

where the parameters $a_1 = 0.2$, $a_2 = 0.72$ and $a_3 = 0.81$. E_{xc}^{LSDA} stands for the exchange energy obtained from local spin density approximation whereas E_x^{GC} and E_c^{GC} are the gradient corrections for exchange and correlation respectively.

ωB97XD which includes empirical dispersion and is the latest functional from Head-Gordon and Coworkers, is a long-range corrected (LC) hybrid density functional. It uses 100% Hartree-Fock exchange for long range electron-electron interactions and 22% for short-range exact exchange which leads it to eliminate the problem of failing in long-range charge transfer excitations between a donor and acceptor.

PBE1PBE uses 25% exact exchange and 75% DFT exchange, and is also known in the literature as PBE0.

M06-2X [28], parametrized only for non-metals, is one of the variations of M06 hybrid meta-exchange correlation functional of Truhlar and Zhao. Its usage areas include thermochemical properties and excited state calculations.

3.2. Basis Sets

Basis sets are sets of non-orthogonal one-particle functions used to generate molecular orbitals, which are expressed as a linear combination with coefficients to be determined. They both define wavefunctions and take an important part in solving the Schrödinger's equation.

Developed by John Pople and popularized by the Gaussian set of programs, the most widely used basis sets in quantum chemical calculations are 3-21G, 6-21G, 6-31+G, 6-31G* and 6-311G*. The functions are splitted meaning the first number demonstrates the primitives in the core functions, and the numbers after the hyphen denote the number of primitives used in the valence functions. Two numbers after the hyphen express valence double-ζ basis, and three numbers after the hyphen represent valence triple-ζ basis. Polarization and diffuse functions can also be attached in order to expand the basis set, have more mathematical flexibility in calculations and define the quantum mechanical system better. + sign in basis sets stands for diffuse functions and * sign represents polarization functions on non-hydrogen atoms and ** denotes the polarization functions are appended to the light atoms i.e. hydrogen and helium.

The basis set used in this study is 6-311G*. 6-31G* or 6-31G(d) is 6-31G with added d polarization functions on non-hydrogen atoms and 6-311G* is a split valence triple-ζ basis, it adds one Gaussian type orbital (GTO) to 6-31G*.

3.3. Time Dependent Density Functional Theory

Time Dependent Density Functional Theory (TD-DFT) is a quantum mechanical approach that is used for calculating the electronic excited states. The Hamiltonian is described as:

$$\hat{H} = \hat{T}(\underline{r}) + \hat{W}(\underline{r}) + \hat{V}_{ext}(\underline{r}, t) \tag{3.13}$$

where $\hat{T}(\underline{r})$ represents the kinetic energy of electrons, $\hat{W}(\underline{r})$ denotes the Coulomb interaction between the electrons and $\hat{V}_{ext}(\underline{r}, t)$ is the time-dependent potential that the electrons are under the influence of. The external potential defines the excited state hence the potential effects must be known when calculating the properties of the excited state.

The Hohenberg-Kohn Theorem is applied to a variational principle involving the action

$$A = \int_{t_0}^{t_1} \langle \psi(t) | i\frac{\delta}{\delta t} - \hat{H} | \psi t \rangle dt \tag{3.14}$$

and up to a time-dependent constant, the wavefunction is decided:

$$\psi(r_1, r_2, ..., r_N, t) = \psi[\rho](t) e^{i\alpha(t)} \tag{3.15}$$

To the action in Equation 3.14, the phase factor is added as a constant:

$$A[\rho] = \int_{t_0}^{t_1} \langle \tilde{\psi}[\rho](t) | i\frac{\delta}{\delta t} - \hat{H}(t) | \tilde{\psi}[\rho](t) \rangle dt + \alpha(t_1) - \alpha(t_0) = A[\rho] + constant \tag{3.16}$$

and A(ρ) can be expressed as:

$$A[\rho] = B[\rho] - \int dr \int_{t_0}^{t_1} (r,t)\rho(r,t)dt \tag{3.17}$$

where B[ρ] is independent of the external potential. If we assume an independent system which has a property as:

$$\rho(r,t) = \sum_i f_i |\psi_i(r,t)|^2 \tag{3.18}$$

Therefore, B[ρ] can be expressed as:

$$B[\rho] = \sum_i f_i \int_{t_0}^{t_1} \langle \psi_i(t)|i\frac{\delta}{deltat} - \frac{1}{2}\nabla_i^2|\psi_i(t)\rangle dtv - \frac{1}{2}\int_{t_0}^{t_1} dt \int\int dr_1 dr_2 \frac{\rho(r_1,t)\rho(r_2,t)}{|r_1 - r_2|} - A_{xc}[\rho] \tag{3.19}$$

where $A_{xc}[\rho]$ represents both the exchange and correlation. Applying the variational principle to Equation 3.18 with constraint:

$$\rho(r,t) = \sum_i f_i |\psi_i(r,t)|^2 = \sum_i^N |\psi_i(r,t)|^2 \tag{3.20}$$

the time-dependent Kohn-Sham equation below is acquired:

$$[-\frac{1}{2}\nabla^2 + V_{eff}(r,t)]\psi_i(r,t) = i\frac{\delta}{\delta t}\psi_i(r,t) \tag{3.21}$$

$$V_{eff}(r,t) = V_H(r,t) + V_{xc}(r,t) + V_{ext}(r,t) \tag{3.22}$$

and now the unknown term is the time-dependent exchange potential, and all exchange and correlation effects in TD-DFT are collected as:

$$V_{xc}[\rho](r,t) = \frac{\delta A_{xc}[\rho]}{\delta \rho(r,t)} \tag{3.23}$$

In time-dependent density functional theory equations, there is not any approximations. As the exchange correlation action function is not known, approximations should be conducted. The adiabatic approximation (AA) is:

$$V_{xc}[\rho](r,t) = \frac{\delta A_{xc}[\rho]}{\delta \rho(r,t)} \sim \frac{\delta E_{xc}[\rho]}{\delta \rho(r)}|_{\rho=\rho(r,t)} \tag{3.24}$$

which means if the electron density changes, the exchange and correlation potential changes instantaneously.

3.4. Conformer Search

Energy in a molecule is defined as a function of the degrees of freedom. Conformational energy searching of a molecule is applied in order to compute all of the energetically desired conformations. To put it in other words, this is mathematically equivalent to addressing all of the minima of the energy function. An energy surface includes energy barriers, energy minima and saddle points. Molecular mechanics energy approximations have more accurate results mostly in and around the minima points. The lowest energy minima are inclined to be the most populated [29].

3.5. Geometries

Geometry optimization is an approach to forecast the three-dimensional adjustments of the atoms in a molecule by means of depreciation of a model energy. As a consequence of geometry optimization, the tendency of atoms and molecules to group into stable and larger structures can be explained, at least in principle.

3.6. Distortion Energies

Distortion energy is significant while deciding the planarity of the molecule. It is calculated as the total energy difference between the relaxed geometry and the constrained conformation which has dihedral angles between the donor and the acceptor constrained to zero. The neutral molecules are optimized and the dihedral angles of

this neutral conformation are monitored. Then, the dihedral angles of the relaxed geometry are constrained to zero thus, the constrained geometry is obtained [30]. Finally, single point calculations are performed.

3.7. Reorganization Energies

Hopping-type and band-type charge transport are two ways of charge transport in organic materials [31]. In π-conjugated molecules, there is hopping-type charge transfer. Internal reorganizations, controlling the charge transfer mobility, play a significant role in choosing the charge transfer characteristics of organic substances. Conjugation length and degree are two major factors on which reorganization energy is dependent [32].

When an electron is removed or attached, inner reorganizational energy is created with the modifications in the geometry of the molecule. The change in conformations and the energies of the molecule in the cation and anion states should be calculated in order to determine the reorganizational energy.

The difference of the energy needed to go with the neutral conformation to the cation state E_+^* and the energy of the cation E_+ creates the λ_+ part of the reorganization energy. The difference of the energy needed for cation geometry to have neutral state E_0^* and the energy of the neutral E_0 creates the λ_0 part of the reorganization energy. And the hole transfer reorganizational energy is the sum of λ_+ and λ_0. Equation 3.25 demonstrates the formula for the hole transfer reorganizational energy Figure 3.1 is a graphical illustration of this formula.

$$\lambda = \lambda_0 + \lambda_+ = (E_0^* - E_0) + (E_+^* - E_+) \tag{3.25}$$

For the electron transfer reorganizational energy, we need to perform a similar calculation as above. The difference between the energy required for the anion state with the neutral conformation E_-^* and the energy of the anion state E_- creates the

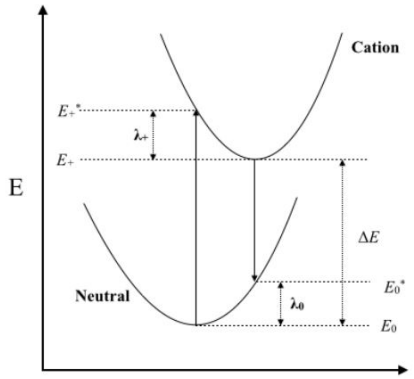

Figure 3.1. Internal reorganization energy $\lambda_+ + \lambda_0$ for Hole Transfer, and Adiabatic Ionization Energy, ΔE

λ_- part of the reorganizational energy. The difference between the energy needed for anion geometry to have neutral state E_0^* and the energy of the neutral state E_0 creates the λ_0 part of the reorganizational energy. Equation 3.26 demonstrates the formula for the electron transfer reorganizational energy and Figure 3.2 is a graphical illustration of this formula.

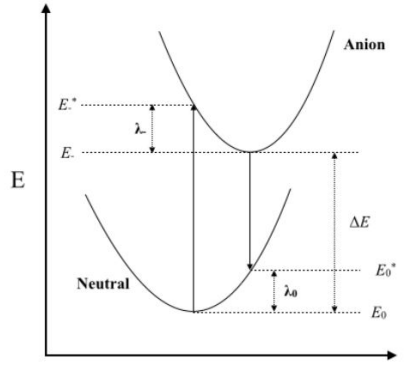

Figure 3.2. Internal reorganization energy $\lambda_- + \lambda_0$ for Electron Transfer, and the Adiabatic Ionization Energy, ΔE

$$\lambda = \lambda_0 + \lambda_- = (E_0^* - E_0) + (E_-^* - E_-) \tag{3.26}$$

3.8. Natural Transition Orbitals

The description of electronically excited states is framed in terms of excitation amplitudes depending on a set of ground state orbitals. For instance, in the configuration interaction singles (CIS) methodology to excited states, the many electron space are composed of all single particle-hole excitations (singles) from the ground state [33].

Assume the CIS approximation, which is equal to the Tamm–Dancoff approximation of TD-DFT. The outcome of a self-consistent field (SCF) computation on the ground state is an orthogonal set of N_o occupied spin orbitals, Ψ_i , and a set of N_v unoccupied spin orbitals, Ψ'_a . Consider that $N_v \geq N_o$, as is usually the case. The consistent quantity combined with the electronic excitation is the single particle transition density matrix T, a rectangular $N_o \times N_v$ matrix pairing the ground state Ψ_0 with the excited state Ψ_{ex} [33],

$$T_{ia} = \sum_{\sigma} < \Psi_{ex}|c'_{i\sigma}c_{a\sigma}|\Psi_0 > \tag{3.27}$$

where the index i represents occupied orbitals in the set Ψ, the index a represents the virtuals in the set Ψ' and σ shows the spin index.

If two new sets of orbitals which are defined by unitary transformations are created, the result will be;

$$(\phi_1, \phi_2, ..., \phi_{N_o}) = (\psi_1, \psi_2, ..., \psi_{N_o})\, U \tag{3.28}$$

and

$$(\phi'_1, \phi'_2, ..., \phi'_{N_o}) = (\psi'_1, \psi'_2, ..., \psi'_{N_o})\, V \tag{3.29}$$

If eigenvalue equations are solved, U and V matrices are determined,

$$TT'u_i = \lambda_i u_i, i = 1, 2, ..., N_o \tag{3.30}$$

$$T'Tv_i = \lambda'_i v_i, i = 1, 2, ..., N_v \tag{3.31}$$

with

$$U = (u_1, u_2, ..., u_{N_o}) \tag{3.32}$$

$$V = (v_1, v_2, ..., v_{N_o}) \tag{3.33}$$

The three properties of the newly formed orbitals ϕ and ϕ' are listed as follows:

- In order of decreasing magnitude, λ_i and λ'_i are ordered as;

$$1 \geq \lambda_i \equiv \lambda'_i \geq 0, i = 1, ..., N_o \tag{3.34}$$

and

$$\sum_{i}^{N_o} \lambda_i = 1 \tag{3.35}$$

- The eigenvectors $u_{N_o+1}...v_{N_v}$ will equal to 0 as eigenvalues.
- The transition density is diagonal in terms of newly formed orbitals.

$$|[U'TV]_{ij}| = \sqrt{\lambda_i \delta_{ij}} \tag{3.36}$$

TT' and $T'T$ are diagonalized in order to obtain virtual and occupied natural transition orbitals (NTO) and each occupied orbital is coupled with single virtual orbital; the transition density does not change.

4. RESULTS

4.1. Benchmark Calculations

The 4 different donors studied for benchmark calculations are benzo [1,2-b:4,5-b'] dithiophene (BDT), 3,3'-difuoro-2,2'-bithiophene (diF2T), naphtho [1,2-b:5,6-b'] dithiophene (NDT) and thieno[3,2-b] thiophene (TT). The acceptor used in benchmark calculations is 2-propyl-5,6-difluorobenzo[d][1,2,3]triazole (ffTAZ) [21].

The narrow bandgap (NBG) indacenodithieno[3,2-b]thiophene (IDTT)-based small molecules, such as ITIC (optical bandgap (E_g^{opt}= 1.59 eV), ITIC-Th, (E_g^{opt}=1.60 eV) and IT-4F, (E_g^{opt}=1.52 eV) have become one of the most successful NFA series and excellent photovoltaic performance with power conversion efficiency (PCE) exceeding 13% has been realized [21]. Because ITIC series acceptors have narrow bandgaps (E_g^{opt}<1.60 eV), donor molecules are preferred with wide bandgaps (E_g^{opt}>1.80 eV) [21]

The optical band gap is 1.83 eV for P-diF2T, 1.85 eV fot P-TT, 1.90 eV for P-BDT and 2.05 eV for P-NDT meaning they possess wide band gaps [21]. The reasons of choosing these molecules for benchmark calculations are that their power conversion efficiencies (PCEs) are higher than 7% and all of them demonstrate temperature-dependent aggregation behaviour in solution [21]. Figure 4.1 demonstrates the donors used for benchmark calculations while Figure 4.2 shows the structures of benchmark molecules.

Seferos et al. (2013) have used the B3LYP/6-311G* methodology in order to calculate HOMO, LUMO and energy band gaps in five different ways [3]. The geometry was optimized at the neutral singlet ground state and all remaining computations were performed using this geometry. Three subsequent single point energy calculations were performed on the oxidized (+1) doublet (the optimization energy of the cation molecule), the reduced (−1) doublet (the optimization energy of the anion molecule), and the neutral triplet state [3].

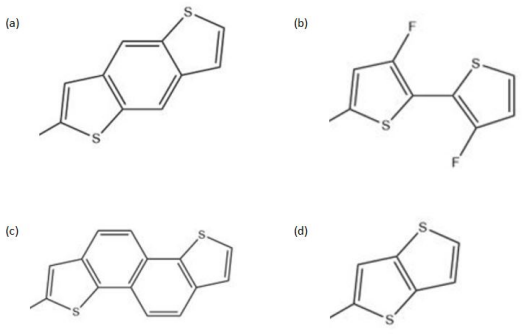

Figure 4.1. Structures of Donors: (a) BDT (b) diF2T (c) NDT (d) TT

Figure 4.2. Structures of Benchmark Molecules: (a) P-BDT (b) P-diF2T (c) P-NDT (d) P-TT

For the four molecules studied in benchmark calculations, the geometries were optimized using neutral ground, oxidized (+1) doublet, reduced (-1) doublet, neutral triplet states and TD-DFT calculations from the neutral singlet state hence, the HOMO energies and the LUMO energies were calculated. Then, the difference between the HOMO energies and the LUMO energies were calculated and fundamental band gaps were obtained.

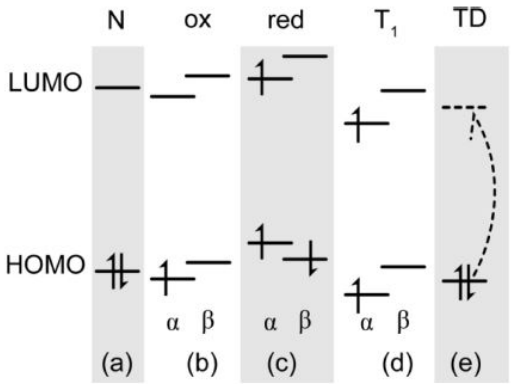

Figure 4.3. Representation of five different states: (a) Neutral Ground State (b) Oxidized Doublet State (c) Singly Reduced Doublet State (d) Neutral Triplet State (e) TD-DFT State [3]

The band gaps of the molecules under investigation have been obtained in two different ways. The first one is by calculating the fundamental band gaps by using the energy differences between the HOMO and the LUMO from neutral ground, oxidized (+1) doublet, reduced (-1) doublet and neutral triplet states. The second one is by calculating the vertical excitation energy of lowest lying singlet excited state ($S_0 \rightarrow S_1$) by using the TD-DFT calculations.

Benchmark calculations were performed using the 6-311G* basis set and the B3LYP, PBE0, ωB97XD and M06-2X functionals. Geometry optimizations were conducted by using the B3LYP/6-311G* methodology and other methods were carried out as single point calculations. The conformation search was performed on these four molecules: the positions of donor-acceptor molecules were evaluated in terms of syn or anti conformations in which electronegative atoms of donors and acceptors stay in the

same direction is defined as syn conformation (uu or dd) whereas the opposite direction is defined as anti conformation (du or ud). The letter u symbolizes up while the letter d symbolizes down as directions.

Table 4.1 demonstrates the experimental HOMO, LUMO and E_g values in eV for benchmark molecules P-BDT, P-diF2T, P-NDT and P-TT [21].

Table 4.1. Experimental HOMO, LUMO and E_g (eV) Values of P-BDT, P-diF2T, P-NDT and P-TT [21]

Molecules	**HOMO**	**LUMO**	E_g
P-BDT	-5.39	-2.87	1.90
P-diF2T	-5.41	-3.00	1.83
P-NDT	-5.41	-2.73	2.04
P-TT	-5.35	-2.93	1.85

4.1.1. Geometries

A conformation search was conducted for P- polymer before the selected donor parts were attached. Figure 4.4 shows the geometric structure of P- polymer. The Hartree electronic energies, relative electronic energies and total dipole moments were calculated and displayed in Table 4.2 for all possible conformations of P- polymer. The duud (down-up-up-down) conformation was selected as the best one since its both relative electronic energy and total dipole moment is the smallest among the others. Another reason for its stability is that the duud conformation has hydrogen bonding because N and H atoms are close to each other. The geometric structures of all conformations are displayed in Figure 4.5.

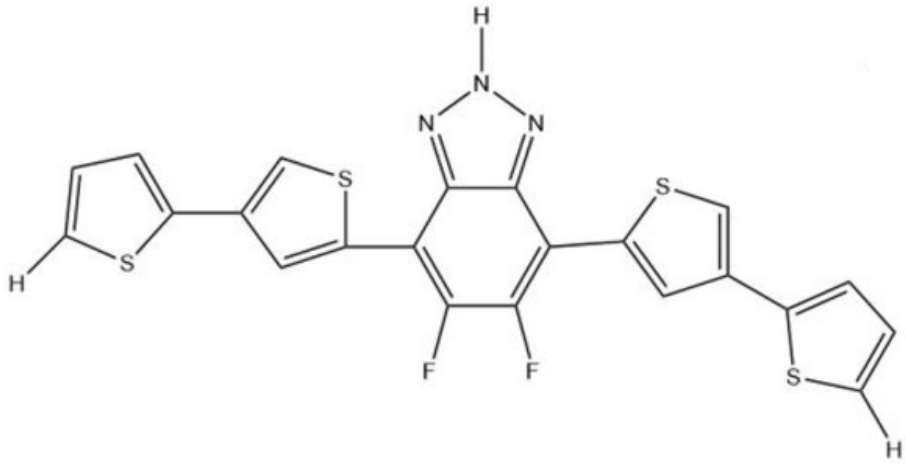

Figure 4.4. Geometry of P- Polymer

Table 4.2. Electronic Energies (Hartree), Relative Electronic Energies (kcal/mol) and Total Dipole Moment of the Conformations of P- Polymer, B3LYP/6-311G*

Name	E_{el}	**Rel.** E_{el}	**Dipole**
dddd	-2801.9536373	1.77	4.19
dddu	-2801.9534734	1.67	3.30
ddud	-2801.9522451	0.90	3.42
dduu	-2801.9525738	1.11	2.39
dudd	-2801.9522559	0.91	3.47
duud	-2801.9508087	0.00	1.60
duuu	-2801.9511101	0.19	1.77
uddd	-2801.9534780	1.68	3.56
uddu	-2801.9533295	1.58	2.50
uduu	-2801.9523929	0.99	1.84
uudd	-2801.9525893	1.12	2.70
uudu	-2801.9523929	0.99	1.87
uuud	-2801.9511101	0.19	2.02
uuuu	-2801.9513969	0.37	1.91

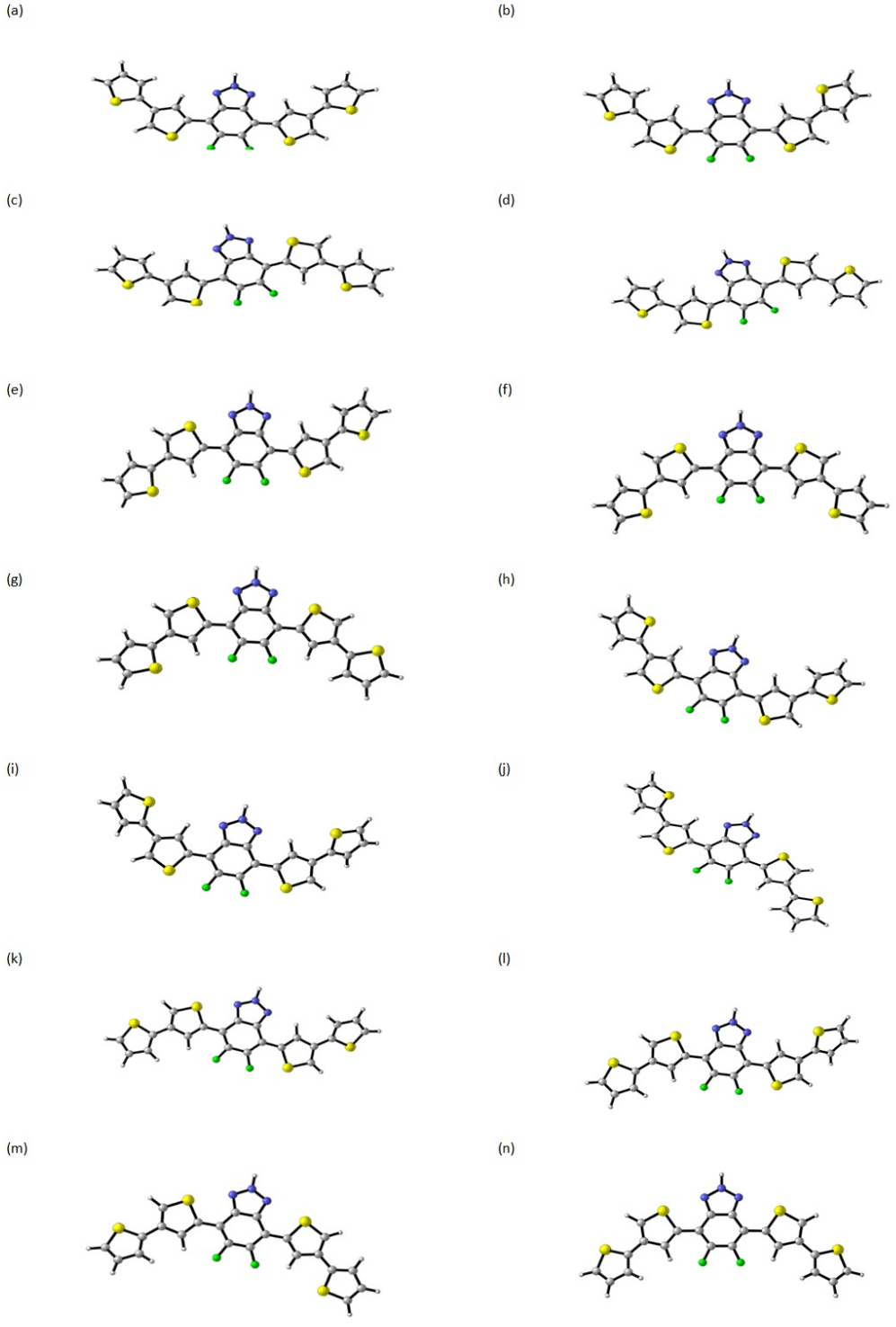

Figure 4.5. All Possible Conformations of P- Polymer: (a) dddd (b) dddu (c) ddud (d) dduu (e) dudd (f) duud (g) duuu (h) uddd (i) uddu (j) uduu (k) uudd (l) uudu (m) uuud (n) uuuu (B3LYP/6-311G*)

HOMO, LUMO and electronic energy band gap values for conformations of P-BDT at B3LYP/6-311G* level of theory are displayed in Table 4.3 and the geometric structures of these conformations are shown in Figure 4.5. The calculations demonstrate the fact that du (down-up) conformation is the best one for P-BDT since its relative electronic energy and total dipole moment is the smallest among the others.

Table 4.3. Electronic Energies (Hartree), Relative Electronic Energies (kcal/mol) and Total Dipole Moment of the Conformations of P-BDT, B3LYP/6-311G*

Name	E_{el}	**Rel.** E_{el}	**Dipole**
P-BDT-dd	-3981.9390907	0.43	1.77
P-BDT-du	-3981.9397732	0.00	1.67
P-BDT-ud	-3981.9396328	0.09	1.79
P-BDT-uu	-3981.9391675	0.38	1.72

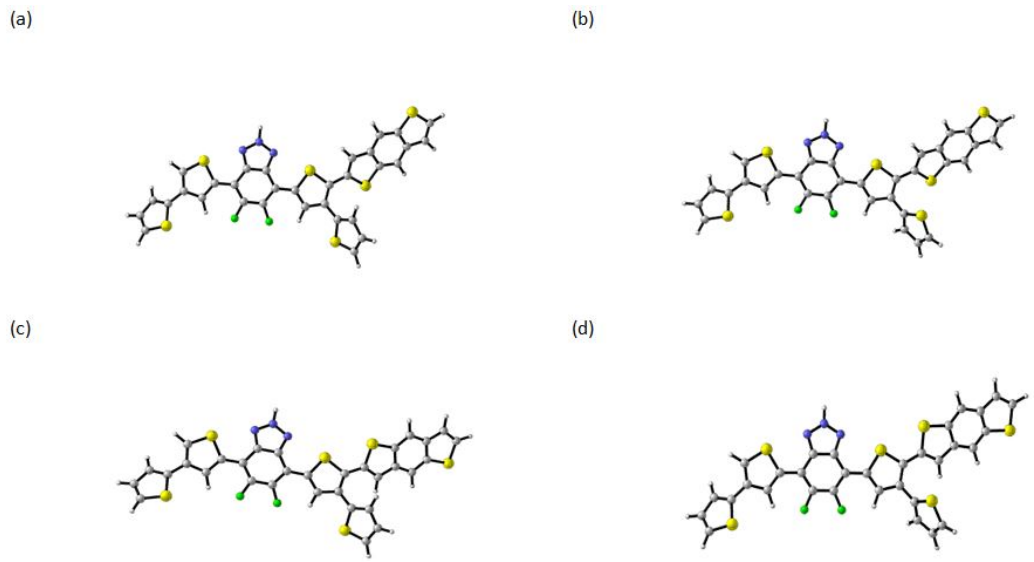

Figure 4.6. All Possible Conformations of P-BDT: (a) dd (b) du (c) ud (d) uu

HOMO, LUMO and electronic energy band gap values for conformations of P-diF2T at B3LYP/6-311G* level of theory are displayed in Table 4.4 and the geometric structures of these conformations are shown in Figure 4.6. The calculations demonstrate the fact that du (down-up) conformation is the best one for P-diF2T since its relative electronic energy and total dipole moment is the smallest among the others.

Table 4.4. Electronic Energies (Hartree), Relative Electronic Energies (kcal/mol) and Total Dipole Moment of the Conformations of P-diF2T, B3LYP/6-311G*

Name	E_{el}	**Rel.** E_{el}	**Dipole**
P-diF2T-dd	-4104.2095031	0.18	1.56
P-diF2T-du	-4104.2097845	0.00	1.53
P-diF2T-ud	-4104.2093582	0.27	1.79
P-diF2T-uu	-4104.2093591	0.27	1.79

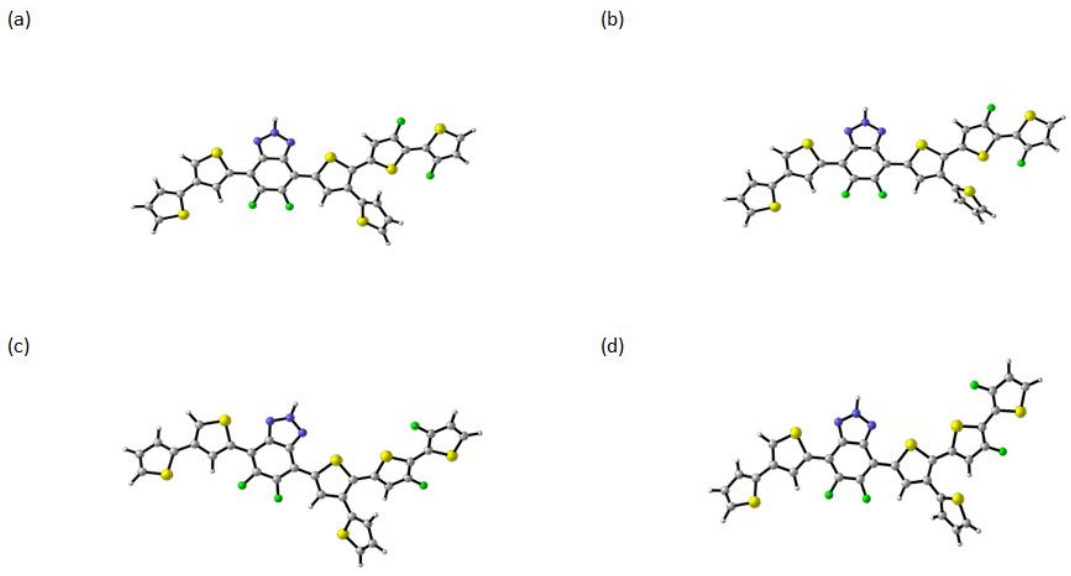

Figure 4.7. All Possible Conformations of P-diF2T: (a) dd (b) du (c) ud (d) uu

HOMO, LUMO and electronic energy band gap values for conformations of P-NDT at B3LYP/6-311G* level of theory are displayed in Table 4.5 and the geometric structures of these conformations are shown in Figure 4.7. The calculations demonstrate the fact that du (down-up) conformation is the best one for P-NDT since its relative electronic energy and total dipole moment is the smallest among the others.

Table 4.5. Electronic Energies (Hartree), Relative Electronic Energies (kcal/mol) and Total Dipole Moment of the Conformations of P-NDT, B3LYP/6-311G*

Name	E_{el}	**Rel.** E_{el}	**Dipole**
P-NDT-dd	-4135.616787	0.12	2.04
P-NDT-du	-4135.6169800	0.00	1.75
P-NDT-ud	-4135.6163292	0.41	2.71
P-NDT-uu	-4135.6169824	0.00	1.80

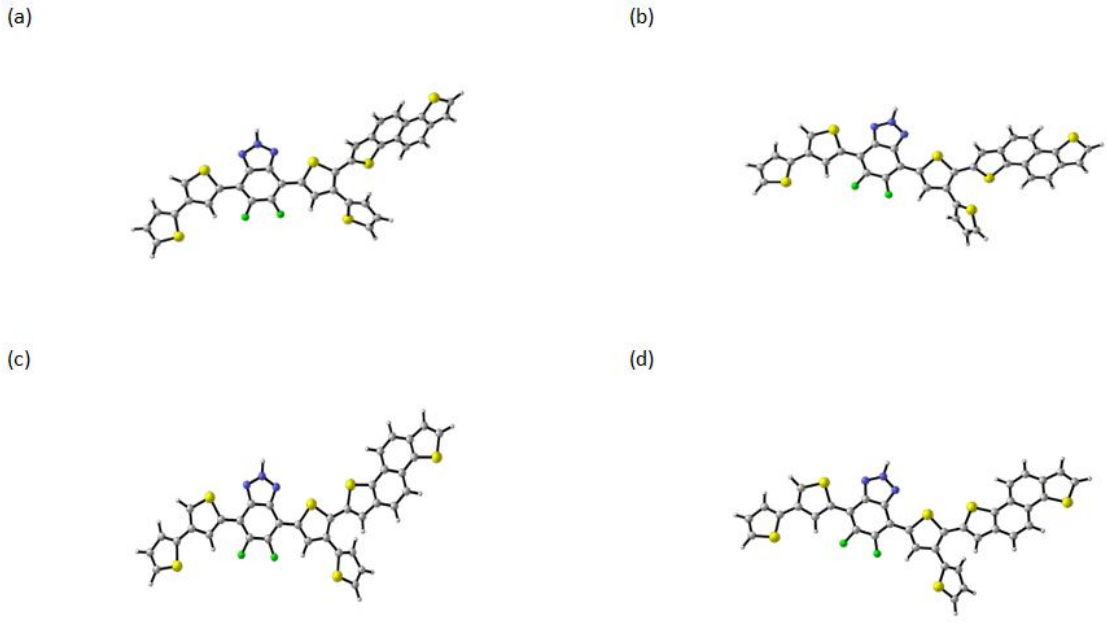

Figure 4.8. All Possible Conformations of P-NDT: (a) dd (b) du (c) ud (d) uu

HOMO, LUMO and electronic energy band gap values for conformations of P-TT at B3LYP/6-311G* level of theory are displayed in Table 4.6 and the geometric structures of these conformations are shown in Figure 4.8. The calculations demonstrate the fact that du (down-up) conformation is the best one for P-TT since its relative electronic energy and total dipole moment is the smallest among the others.

Table 4.6. Electronic Energies (Hartree), Relative Electronic Energies (kcal/mol) and Total Dipole Moment of the Conformations of P-NDT, B3LYP/6-311G*

Name	E_{el}	**Rel.** E_{el}	**Dipole**
P-TT-dd	-3828.2567344	0.00	1.94
P-TT-du	-3828.2567338	0.00	1.71
P-TT-ud	-3828.2562295	0.32	2.09
P-TT-uu	-3828.2561435	0.37	1.72

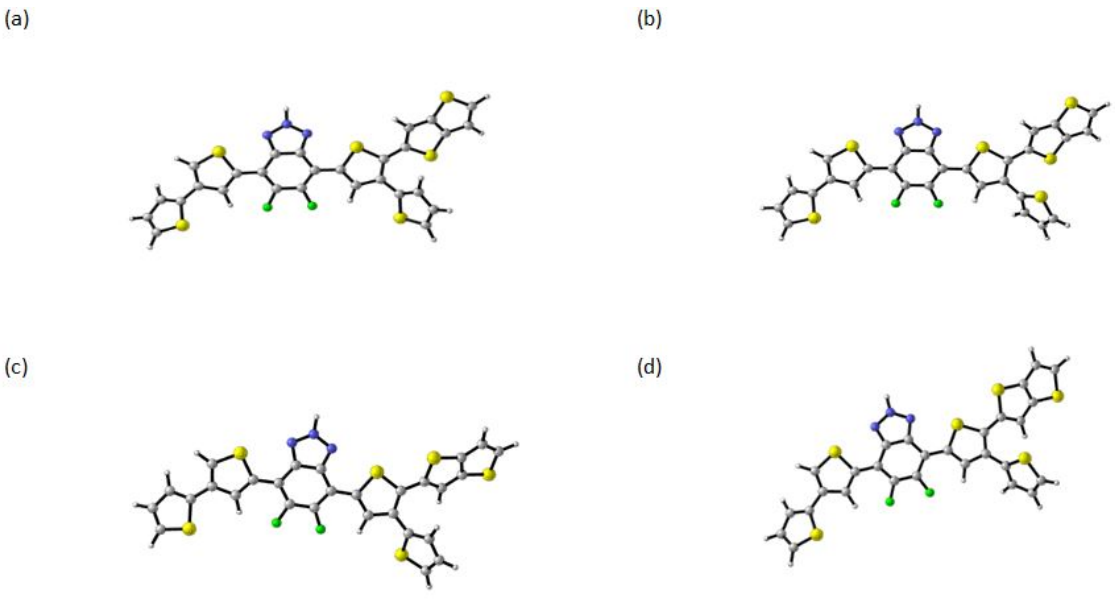

Figure 4.9. All Possible Conformations of P-TT: (a) dd (b) du (c) ud (d) uu

4.1.2. Choice of Methodology

Five different methods were performed for P-BDT, P-diF2T, P-NDT and P-TT using B3LYP/6-311G* including neutral ground, oxidized, reduced, triplet and TD-DFT states and HOMO, LUMO and energy band gaps were calculated. After determining the geometry with B3LYP/6-311G*, single point calculations with ωB97XD, PBE0 and M06-2X functionals and 6-311G* basis set were carried out in order to decide the best functional. The absolute percentage errors of HOMO, LUMO and energy band gaps were compared to HOMO, LUMO and energy band gaps of experimental values.

Tables 4.7, 4.8, 4.9 and 4.10 demonstrate five states of P-BDT, P-diF2T, P-NDT and P-TT molecules respectively and their absolute percentage errors from experimental values for four different functionals including B3LYP, ωB97XD, PBE0, M06-2X and 6-311G* basis set. The absolute percentage errors were evaluated in two different ways. The first is for determining the best HOMO and LUMO values and the second is for determining the best electronic band gap value.

Table 4.7 shows that the minimum absolute percentage error of P-BDT for HOMO values is 0.93% and triplet state at B3LYP/6-311G* level of theory. The minimum absolute percentage error of P-BDT for LUMO values is 8.43% and neutral ground state at B3LYP/6-311G* level of theory. Neutral ground state at B3LYP/6-311G* level of theory is the best method since the absolute percentage error for HOMO value of neutral ground state is 1.25% whereas the absolute percentage error for LUMO value of triplet state is 37.08%. The minimum absolute percentage error for electronic band gap is 1.08% and reduced state at PBE0/6-311G* level of theory. For P-BDT molecule, neutral ground state at B3LYP/6-311G* was selected for predicting HOMO and LUMO values whereas reduced state at PBE0/6-311G* was selected for predicting electronic band gap value.

Table 4.8 displays that the minimum absolute percentage error of P-diF2T for HOMO values is 0.50% and neutral ground state at B3LYP/6-311G* level of theory.

The minimum absolute percentage error of P-diF2T for LUMO values is 10.92% and neutral ground state at B3LYP/6-311G* level of theory. The minimum absolute percentage error for electronic band gap is 2.71% and reduced state at PBE0/6-311G* level of theory. For P-diF2T molecule, neutral ground state at B3LYP/6-311G* was selected for predicting HOMO and LUMO values whereas reduced state at PBE0/6-311G* was selected for predicting electronic band gap value.

Table 4.9 demonstrates that the minimum absolute percentage error of P-NDT for LUMO values is 4.17% and neutral ground state at B3LYP/6-311G* level of theory. Neutral ground state at B3LYP/6-311G* level of theory is the best method since the absolute percentage error for HOMO value of neutral ground state is 0.48% whereas the absolute percentage error of P-NDT for LUMO value of triplet state is 43.08%. The minimum absolute percentage error for electronic band gap is 5.06% and TD-DFT state at B3LYP/6-311G* level of theory. For P-NDT molecule, neutral ground state at B3LYP/6-311G* was selected for predicting HOMO and LUMO values whereas TD-DFT state at B3LYP/6-311G* was selected for predicting electronic band gap value.

Table 4.10 demonstrates that the minimum absolute percentage error of P-TT for LUMO values is 11.66% and neutral ground state at B3LYP/6-311G* level of theory. Neutral ground state at B3LYP/6-311G* level of theory is the best method since the absolute percentage error of P-TT for HOMO value of neutral ground state is 1.58% whereas the absolute percentage error for LUMO value of triplet state is 32.59%. The minimum absolute percentage error for electronic band gap is 0.84% and reduced state at B3LYP/6-311G* level of theory. For P-TT molecule, neutral ground state at B3LYP/6-311G* was selected for predicting HOMO and LUMO values whereas reduced state at B3LYP/6-311G* was selected for predicting electronic band gap value.

Table 4.7. Five States of P-BDT Molecule (B3LYP/6-311G*), (ωB97XD/6-311G*), (PBE0/6-311G*), (M06-2X/6-311G*) and Their Absolute Percentage Errors From Experimental Values (eV)

P-BDT	**Functional**	**HOMO**	**% Err**	**LUMO**	**% Err**	**Eg**	**% Err**
Experiment	B3LYP	-5.39		-2.87		1.90	
Ground State	B3LYP	-5.46	1.25	-2.63	8.43	2.83	48.91
Oxidized State	B3LYP	-7.98	48.04	-5.57	93.95	2.41	27.01
Reduced State	B3LYP	-2.59	51.92	-0.79	72.57	1.80	5.04
Triplet State	B3LYP	-5.44	0.93	-3.93	37.08	1.51	20.75
TD-DFT	B3LYP					2.19	15.40
Experiment	ωB97XD	-5.39		-2.87		1.90	
Ground State	ωB97XD	-7.20	33.67	-1.09	62.17	6.12	222.07
Oxidized State	ωB97XD	-9.58	77.75	-4.28	49.04	5.30	179.12
Reduced State	ωB97XD	-4.32	19.92	-2.11	26.56	2.21	16.24
Triplet State	ωB97XD	-7.28	35.12	-5.53	92.75	1.75	7.83
TD-DFT	ωB97XD					2.93	54.06
Experiment	PBE0	-5.39		-2.87		1.90	
Ground State	PBE0	-5.67	5.26	-2.55	11.32	3.13	64.65
Oxidized State	PBE0	-8.20	52.14	-5.54	92.90	2.66	40.23
Reduced State	PBE0	-2.81	47.81	-0.93	67.46	1.88	1.08
Triplet State	PBE0	-5.70	5.77	-4.14	44.21	1.56	17.78
TD-DFT	PBE0					2.34	23.37
Experiment	M06-2X	-5.39		-2.87		1.90	
Ground State	M06-2X	-6.61	22.67	-1.96	31.67	4.65	144.78
Oxidized State	M06-2X	-9.02	67.35	-5.05	76.12	3.97	108.73
Reduced State	M06-2X	-3.66	32.06	-1.50	47.64	2.16	13.64
Triplet State	M06-2X	-6.56	21.65	-4.81	67.62	1.75	8.10
TD-DFT	M06-2X					2.82	48.63

Table 4.8. Five States of P-diF2T Molecule (B3LYP/6-311G*), (ωB97XD/6-311G*), (PBE0/6-311G*), (M06-2X/6-311G*) and Their Absolute Percentage Errors From Experimental Values (eV)

P-diF2T	**Functional**	**HOMO**	**% Err**	**LUMO**	**% Err**	**Eg**	**% Err**
Experiment	B3LYP	-5.41		-3.00		1.83	
Ground State	B3LYP	-5.38	0.50	-2.67	10.92	2.71	48.12
Oxidized State	B3LYP	-7.96	47.14	-5.64	88.05	2.32	26.71
Reduced State	B3LYP	-2.53	53.26	-0.82	72.57	1.71	6.79
Triplet State	B3LYP	-5.37	0.77	-3.93	30.92	1.44	21.25
TD-DFT	B3LYP					2.15	17.38
Experiment	ωB97XD	-5.41		-3.00		1.83	
Ground State	ωB97XD	-7.13	31.73	-1.14	61.98	5.99	227.11
Oxidized State	ωB97XD	-9.52	76.02	-4.34	44.76	5.18	183.06
Reduced State	ωB97XD	-4.26	21.23	-2.14	28.74	2.12	16.05
Triplet State	ωB97XD	-7.20	33.16	-5.47	82.50	1.73	5.52
TD-DFT	ωB97XD					2.79	52.67
Experiment	PBE0	-5.41		-3.00		1.83	
Ground State	PBE0	-5.59	3.38	-2.59	13.68	3.00	64.12
Oxidized State	PBE0	-8.17	50.94	-5.61	86.87	2.56	39.89
Reduced State	PBE0	-2.74	49.28	-0.96	67.86	1.78	2.74
Triplet State	PBE0	-5.62	3.88	-4.12	37.21	1.50	17.83
TD-DFT	PBE0					2.28	24.43
Experiment	M06-2X	-5.41		-3.00		1.83	
Ground State	M06-2X	-6.54	20.95	-2.02	32.76	4.53	147.34
Oxidized State	M06-2X	-8.98	66.05	-5.13	71.09	3.85	110.42
Reduced State	M06-2X	-3.61	33.33	-1.53	48.84	2.07	13.23
Triplet State	M06-2X	-6.48	19.71	-4.77	59.08	1.70	6.88
TD-DFT	M06-2X					2.70	47.70

Table 4.9. Five States of P-NDT Molecule (B3LYP/6-311G*), (ωB97XD/6-311G*), (PBE0/6-311G*), (M06-2X/6-311G*) and Their Absolute Percentage Errors From Experimental Values (eV)

P-NDT	**Functional**	**HOMO**	**% Err**	**LUMO**	**% Err**	**Eg**	**% Err**
Experiment	B3LYP	-5.41		-2.73		2.04	
Ground State	B3LYP	-5.44	0.48	-2.62	4.17	2.82	38.21
Oxidized State	B3LYP	-7.89	45.88	-5.48	100.58	2.42	18.44
Reduced State	B3LYP	-2.61	51.76	-0.79	71.02	1.82	10.85
Triplet State	B3LYP	-5.40	0.13	-3.91	43.08	1.50	26.63
TD-DFT	B3LYP					2.14	5.06
Experiment	ωB97XD	-5.41		-2.73		2.04	
Ground State	ωB97XD	-7.18	32.68	-1.07	60.66	6.10	199.20
Oxidized State	ωB97XD	-9.55	76.54	-4.18	53.24	5.37	163.11
Reduced State	ωB97XD	-4.32	20.18	-2.10	23.20	2.22	8.92
Triplet State	ωB97XD	-7.23	33.62	-5.52	102.09	1.71	16.10
TD-DFT	ωB97XD					2.84	39.26
Experiment	PBE0	-5.41		-2.73		2.04	
Ground State	PBE0	-5.65	4.49	-2.53	7.20	3.12	52.91
Oxidized State	PBE0	-8.12	50.12	-5.44	99.39	2.68	31.27
Reduced State	PBE0	-2.83	47.72	-0.93	65.79	1.89	7.14
Triplet State	PBE0	-5.66	4.57	-4.11	50.65	1.54	24.29
TD-DFT	PBE0					2.29	12.13
Experiment	M06-2X	-5.41		-2.73		2.04	
Ground State	M06-2X	-6.59	21.80	-1.95	28.55	4.64	127.38
Oxidized State	M06-2X	-8.98	65.94	-4.97	81.91	4.01	96.62
Reduced State	M06-2X	-3.67	32.16	-1.49	45.29	2.18	6.69
Triplet State	M06-2X	-6.52	20.51	-4.79	75.35	1.73	15.06
TD-DFT	M06-2X					2.75	34.68

Table 4.10. Five States of P-TT Molecule (B3LYP/6-311G*), (ωB97XD/6-311G*), (PBE0/6-311G*), (M06-2X/6-311G*) and Their Absolute Percentage Errors From Experimental Values (eV)

P-TT	**Functional**	**HOMO**	**% Err**	**LUMO**	**% Err**	**Eg**	**% Err**
Experiment	B3LYP	-5.35		-2.93		1.85	
Ground State	B3LYP	-5.43	1.58	-2.59	11.66	2.85	53.85
Oxidized State	B3LYP	-8.09	51.20	-5.66	93.04	2.43	31.52
Reduced State	B3LYP	-2.46	53.98	-0.63	78.58	1.83	0.84
Triplet State	B3LYP	-5.41	1.05	-3.88	32.59	1.52	17.75
TD-DFT	B3LYP					2.18	17.92
Experiment	ωB97XD	-5.35		-2.93		1.85	
Ground State	ωB97XD	-7.20	34.51	-1.04	64.39	6.15	232.59
Oxidized State	ωB97XD	-9.67	80.71	-4.34	48.09	5.33	188.06
Reduced State	ωB97XD	-4.23	20.91	-1.99	31.94	2.24	20.92
Triplet State	ωB97XD	-7.27	35.91	-5.47	86.78	1.80	2.78
TD-DFT	ωB97XD					2.82	52.26
Experiment	PBE0	-5.35		-2.93		1.85	
Ground State	PBE0	-5.65	5.65	-2.50	14.54	3.15	70.19
Oxidized State	PBE0	-8.31	55.29	-5.62	91.82	2.69	45.29
Reduced State	PBE0	-2.69	49.77	-0.78	73.48	1.91	3.25
Triplet State	PBE0	-5.67	5.95	-4.09	39.45	1.58	14.47
TD-DFT	PBE0					2.31	24.95
Experiment	M06-2X	-5.35		-2.93		1.85	
Ground State	M06-2X	-6.60	23.36	-1.92	34.56	4.68	153.08
Oxidized State	M06-2X	-8.16	52.58	-4.63	57.87	3.54	91.21
Reduced State	M06-2X	-4.08	23.71	-1.90	34.99	2.18	17.66
Triplet State	M06-2X	-5.99	11.89	-4.63	57.87	1.36	26.46
TD-DFT	M06-2X					2.83	52.97

The results in Tables 4.7, 4.8, 4.9 and 4.10 show that the best functional in estimating HOMO and LUMO values is B3LYP in neutral ground state since the absolute percentage errors of B3LYP in ground state are the smallest ones compared to other methods. For estimating electronic energy band gap values the best method is PBE0 in reduced state since its absolute percentage errors from experimental values are 1.08% for P-BDT, 2.74% for P-diF2T, 7.14% for P-NDT and 3.25% for P-TT.

4.1.3. HOMO, LUMO and E_g Values

For predicting HOMO and LUMO values neutral ground state of B3LYP/6-311G* level of theory was chosen. For estimating electronic energy band gaps reduced state of PBE0/6-311G* level of theory was selected.

Table 4.11 displays HOMO, LUMO and electronic energy band gaps of P-BDT, P-diF2T, P-NDT and P-TT at neutral ground state of B3LYP/6-311G* level of theory. The method was chosen in order to predict HOMO and LUMO values so benchmark values for HOMO are in between -5.38 eV and -5.46 eV; and the benchmark values for LUMO are in between -2.59 eV and -2.67 eV.

Table 4.11. HOMO, LUMO and E_g Values of P-BDT, P-diF2T, P-NDT and P-TT for Neutral Ground State in B3LYP/6-311G*

Molecule	**HOMO**	**LUMO**	E_g
P-BDT	-5.46	-2.63	2.83
P-diF2T	-5.38	-2.67	2.71
P-NDT	-5.44	-2.62	2.82
P-TT	-5.43	-2.59	2.85

Table 4.12 displays HOMO, LUMO and electronic energy band gaps of P-BDT, P-diF2T, P-NDT and P-TT at reduced state of PBE0/6-311G* level of theory. The method was chosen in order to predict electronic energy band gap values so benchmark values for E_g are in between 1.78 eV and 1.91 eV.

Table 4.12. HOMO, LUMO and E_g Values of P-BDT, P-diF2T, P-NDT and P-TT for Reduced State in PBE0/6-311G*

Molecule	**HOMO**	**LUMO**	E_g
P-BDT	-2.81	-0.93	1.88
P-diF2T	-2.74	-0.96	1.78
P-NDT	-2.83	-0.93	1.89
P-TT	-2.69	-0.78	1.91

4.1.4. Distortion Energies

There exists 3 dihedral angles for the benchmark molecules following as ϕ_1 representing the dihedral angle which is on the left hand side of the molecule, ϕ_2 representing the dihedral angle which is on middle and ϕ_3 representing the angle which is on the right hand side of the molecule. Figure 4.9 demonstrates the exact positions of the dihedral angles. The distortion energies for 4 benchmark molecules are reported in Table 4.13. Distortion energies of P-BDT, P-diF2T, P-NDT and P-TT are calculated in between 3.08 kcal/mol and 7.03 kcal/mol.

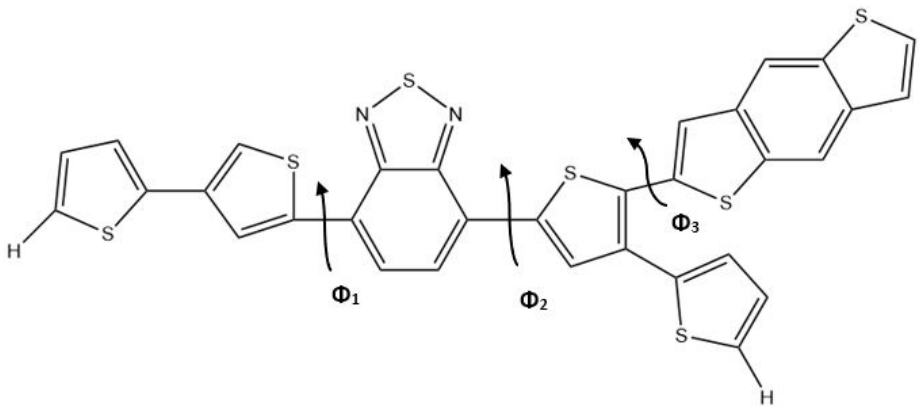

Figure 4.10. Dihedral Angles of Benchmark Molecules

Table 4.13. Dihedral Angles and Total Distortion Energies in kcal/mol for P-BDT, P-diF2T, P-NDT and P-TT Molecules

Molecules	ϕ_1	ϕ_2	ϕ_3	ΔE_{tot}
P-BDT	-3.83	-4.68	44.12	7.03
P-diF2T	2.10	-5.59	37.47	3.08
P-NDT	43.57	-4.07	-3.21	6.41
P-TT	-7.78	-6.71	45.21	6.82

4.1.5. Reorganization Energies

Reorganization energy plays a significant role in deciding about the characteristics of charge mobility and charge transfer in photovoltaic substances. Smaller reorganization energy means higher charge mobility and higher charge transfer rate. Table 4.14 displays the reorganization energies for holes (λ_{hole}) and electrons ($\lambda_{electron}$) of benchmark molecules in meV; adiabatic ionization potential (AIP), adiabatic electron affinity (AEA), vertical ionization potential (VIP) and vertical electron affinity (VEA) of benchmark molecules in eV. The reorganization energies for holes vary in between 255 meV and 342 meV whereas the reorganization energies for electrons are in between 281 meV and 306 meV.

Table 4.14. Reorganization Energies in meV and AIP, AEA, VIP and VEA values in eV for P-BDT, P-diF2T, P-NDT and P-TT

Molecules	λ_{Hole}	$\lambda_{Electron}$	**AIP**	**AEA**	**VIP**	**VEA**
P_BDT	307.92	306.25	6.27	-1.69	6.43	-1.53
P_DİF2T	255.50	284.40	6.29	-1.74	6.39	-1.58
P_NDT	298.25	290.91	6.23	-1.68	6.38	-1.53
P_TT	342.09	281.33	6.28	-1.59	6.46	-1.44

4.1.6. Natural Transition Orbitals

HOMO and LUMO natural transition orbitals of 4 benchmark molecules (P-BDT, P-diF2T, P-NDT and P-TT) are displayed in Figures 4.11, 4.12, 4.13 and 4.14. $S_0 \rightarrow S_1$ excitations were observed from HOMO to LUMO transitions.

In natural transition orbital analysis, it is expected that the electrons gather mostly around the donor part of the molecules in HOMO orbitals whereas the electrons are expected to gather mostly around the acceptor part of the molecules in LUMO orbitals.

Taking a deeper look at the natural transition orbital analysis of HOMO and LUMO orbitals of benchmark molecules, it is clearly seen that the distribution of electrons is denser around the donor parts in HOMO orbitals while the distribution of electrons is denser around the acceptor parts in LUMO orbitals.

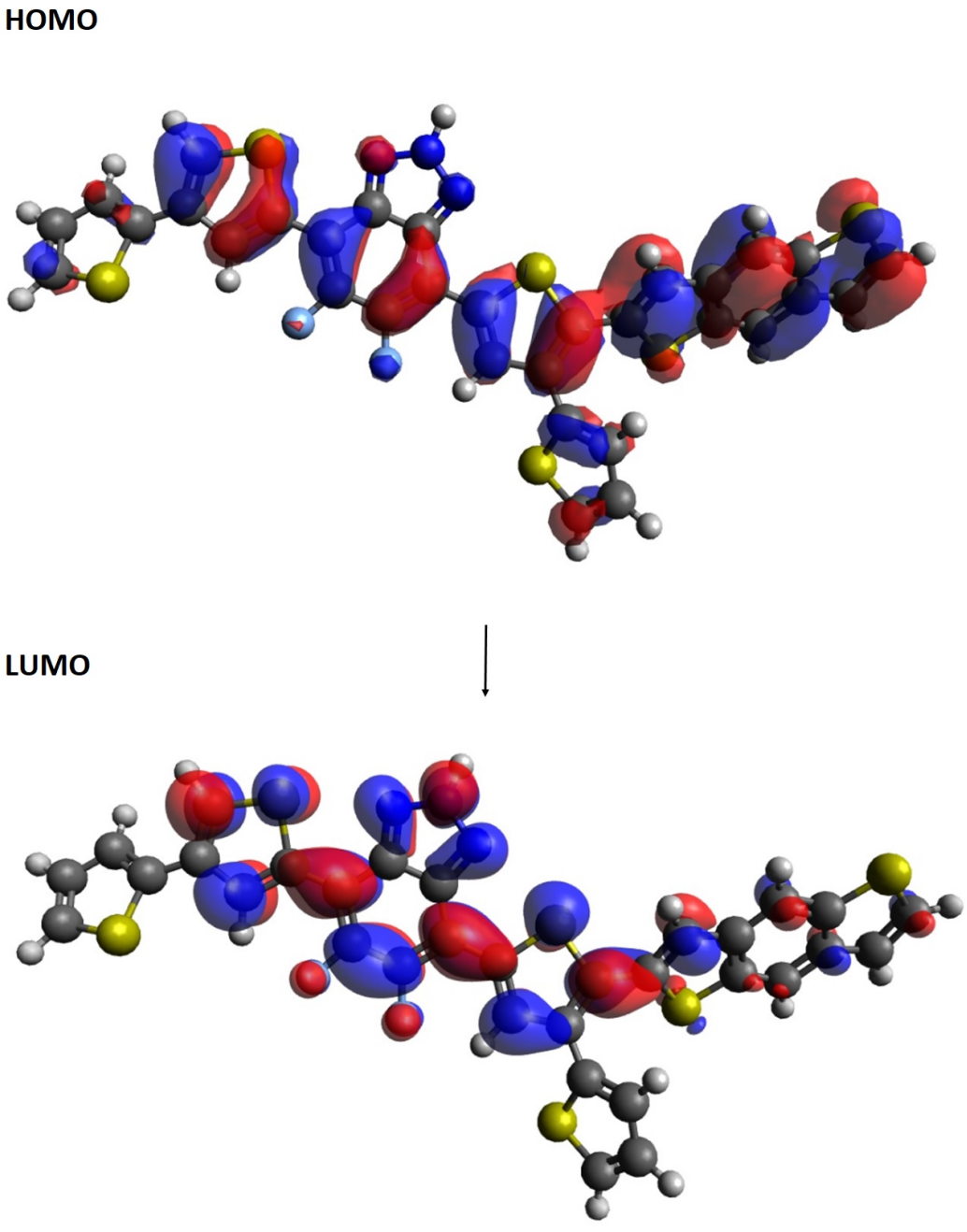

Figure 4.11. Natural Transition Orbitals of P-BDT, B3LYP/6-311G*

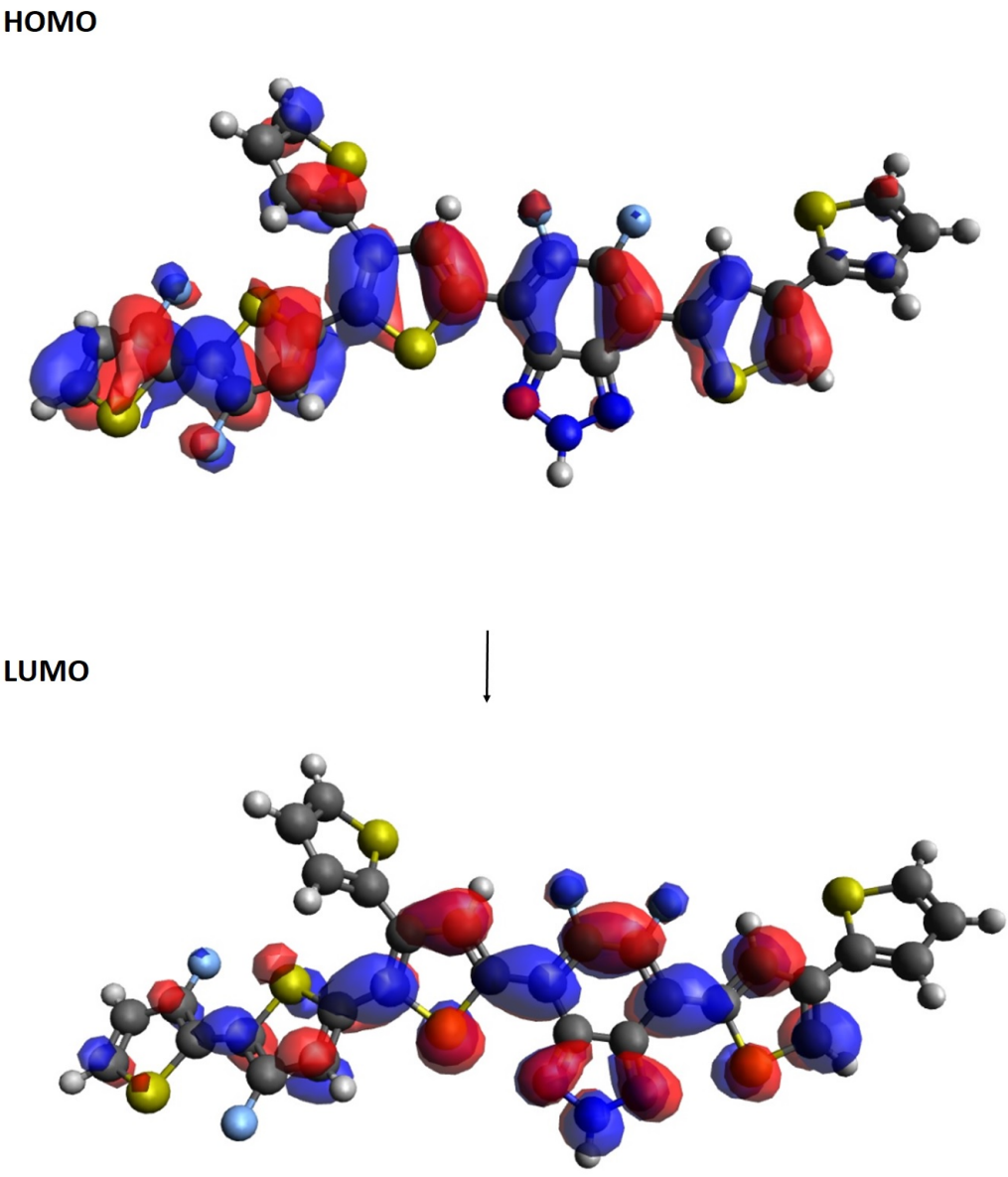

Figure 4.12. Natural Transition Orbitals of P-diF2T, B3LYP/6-311G*

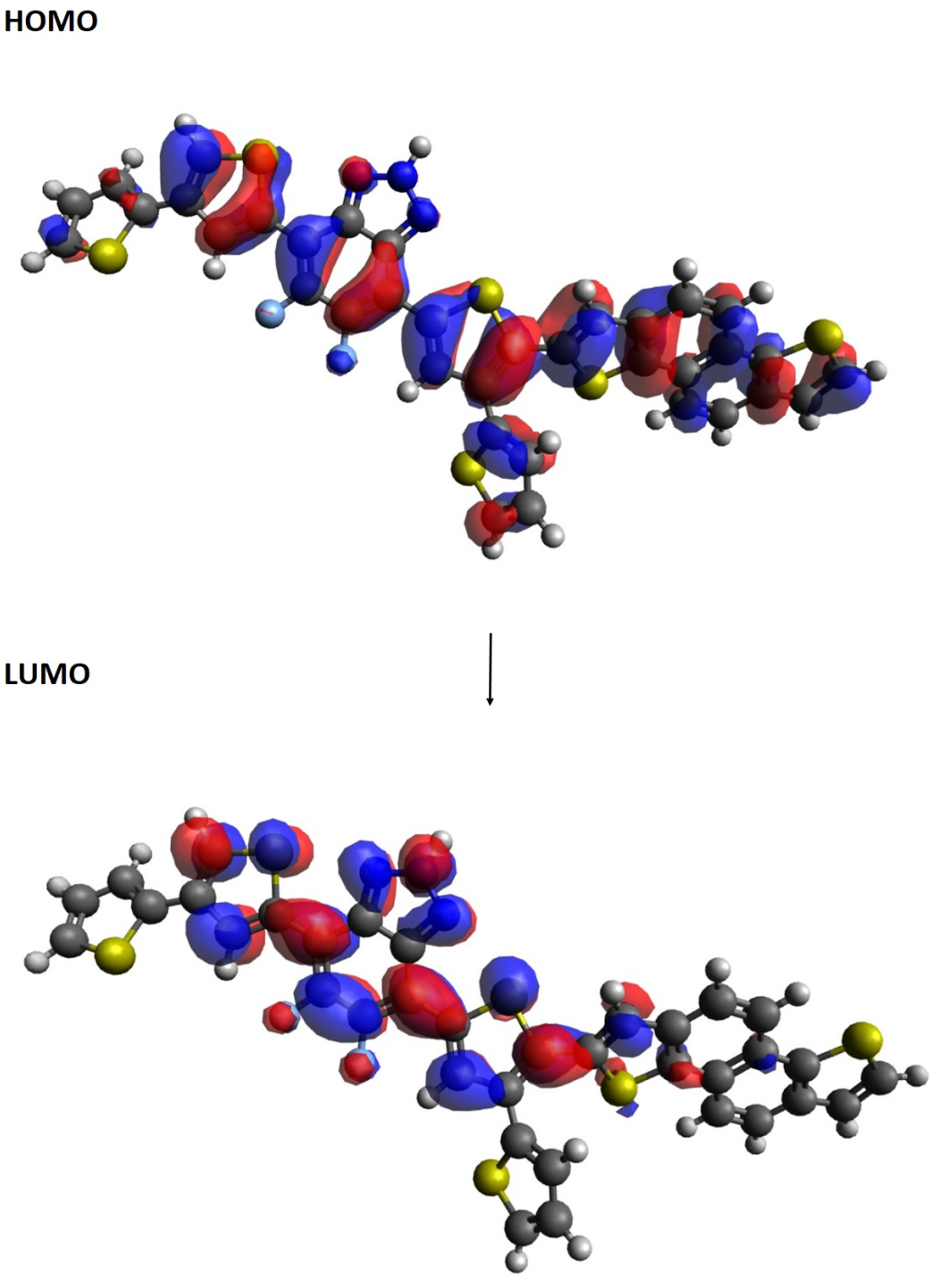

Figure 4.13. Natural Transition Orbitals of P-NDT, B3LYP/6-311G*

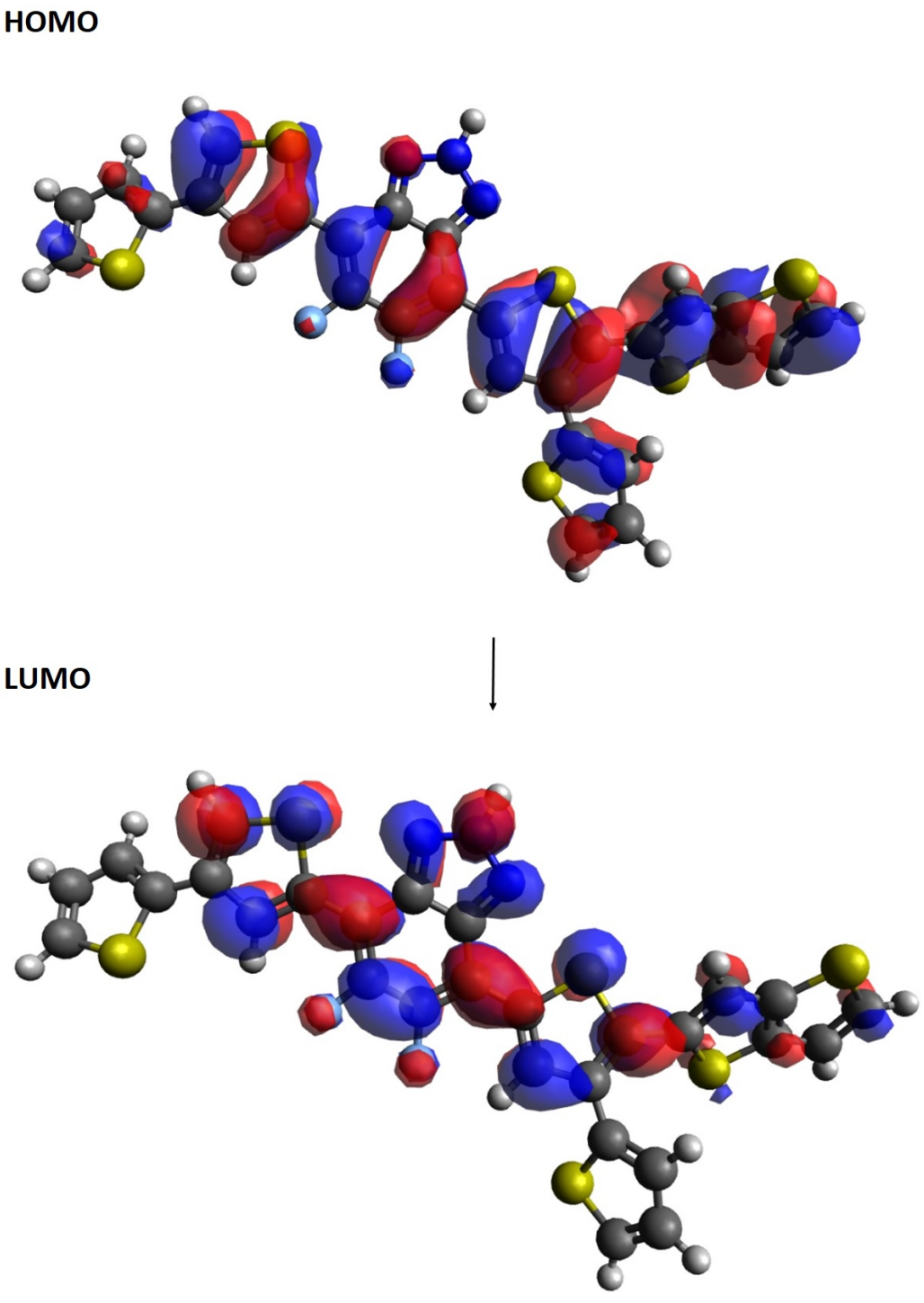

Figure 4.14. Natural Transition Orbitals of P-TT, B3LYP/6-311G*

4.2. Molecules Under Investigation

The 4 different donors studied for benchmarking and 7 different acceptors including benzo [c] [1,2,5] thiadiazole (cop1), [1,2,5] thiadiazolo [3,4-g] quinoxaline (cop2), [1,2,5] thiadiazolo [3,4-d] pyridazine (cop3), [1,2,5] thiadiazolo [3,4-c] pyridine (cop4), [1,2,5] oxadiazolo [3,4-d] pyridazine (cop5), fluorinated naphtho [1,2-c:5,6-c'] bis [1,2,5] thiadiazole (FNTz), fluorinated [2,1,3] benzobisthiadiazole (FBTz) are combined and investigated for 28 different predictions [22, 23].

The 7 different acceptors were chosen based on their similarities in terms of physical and chemical characteristics compared to the acceptor used in benchmark studies. Figure 4.15 displays the geometric structures of 7 different acceptors.

4.2.1. Geometries

All possible conformations of 7 different acceptors before and after attaching the donor parts were evaluated and it was observed that anti (du) conformations were the ones with minimum energies. After conformation search was carried out; HOMO, LUMO and energy band gaps were calculated for the best conformations with neutral ground state at B3LYP/6-311G* and reduced state at PBE0/6-311G*.

4.2.2. HOMO, LUMO and E_g Values

The HOMO values of best molecules should be in between -5.38 and -5.46 eV in B3LYP and LUMO values should be in between -2.59 and -2.67 in B3LYP. The E_g values should be in between 1.78 and 1.91. The molecules whose HOMO, LUMO and E_g values are nearest to the benchmark molecules are FBTz-NDT, FBTz-TT and FNTz-TT.

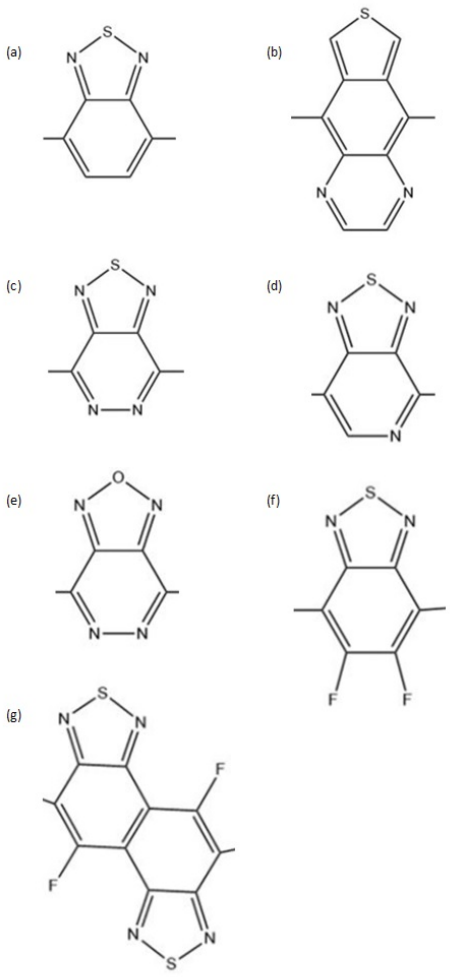

Figure 4.15. Structures of Acceptors: (a) cop1 (b) cop2 (c) cop3 (d) cop4 (e) cop5 (f) FBTz (g) FNTz

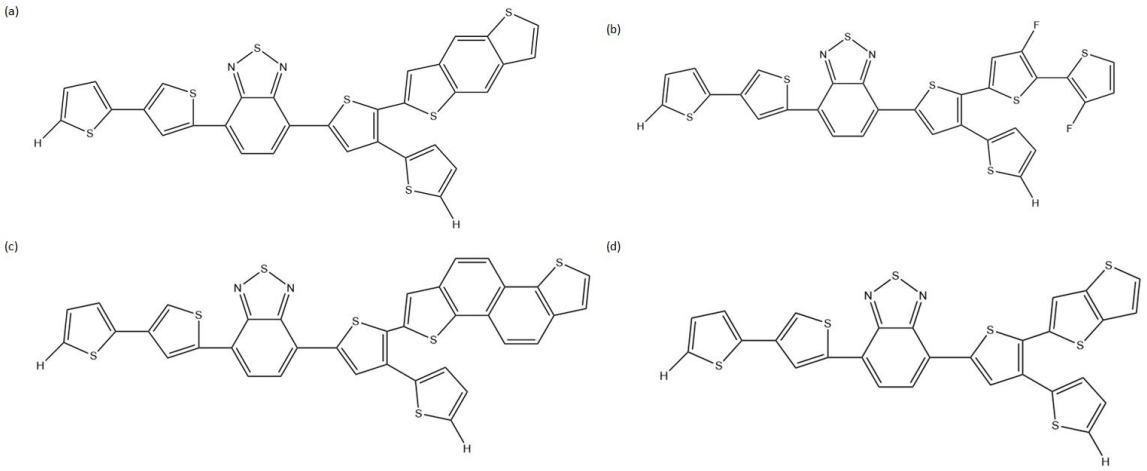

Figure 4.16. Structures of Molecules with cop1 as the Acceptor Unit: (a) cop1-BDT (b) cop1-diF2T (c) cop1-NDT (d) cop1-TT

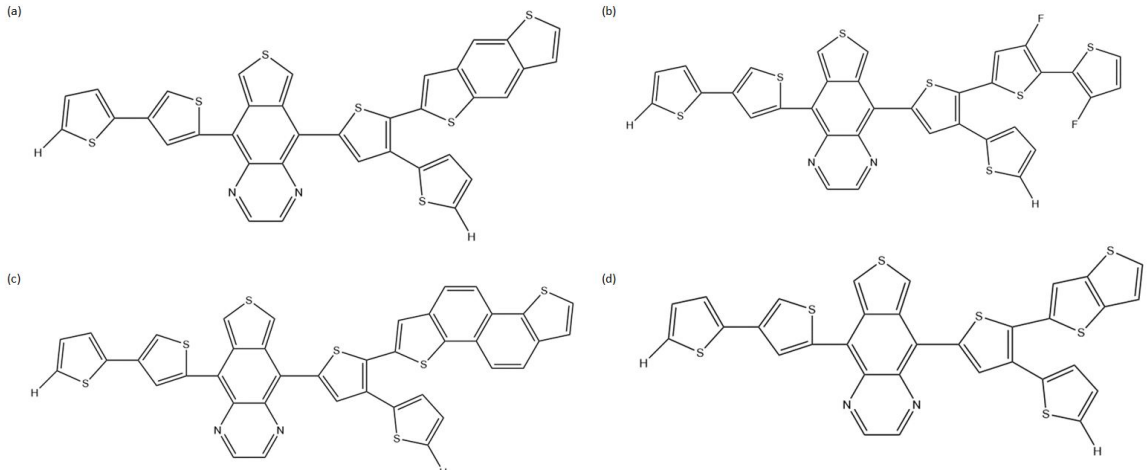

Figure 4.17. Structures of Molecules with cop2 as the Acceptor Unit: (a) cop2-BDT (b) cop2-diF2T (c) cop2-NDT (d) cop2-TT

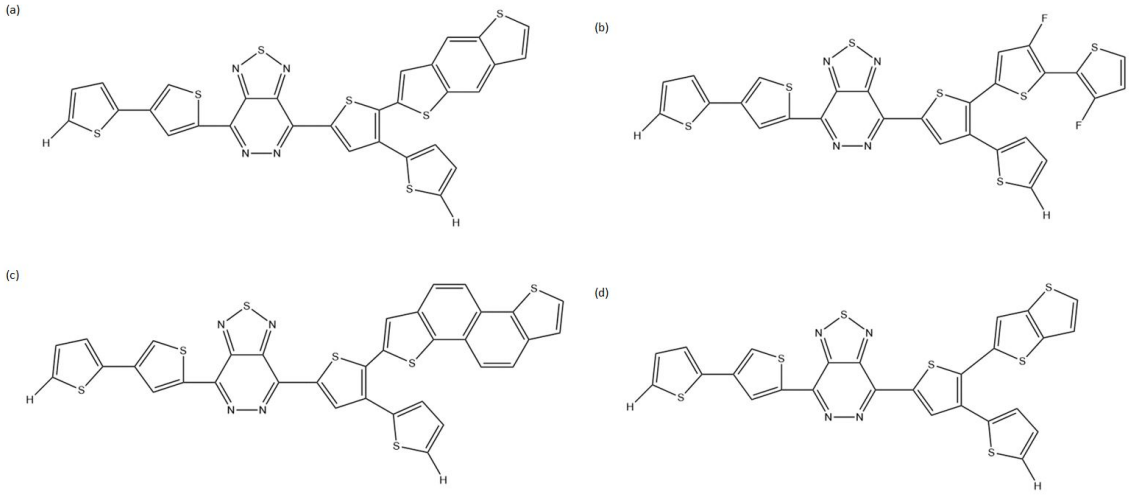

Figure 4.18. Structures of Molecules with cop3 as the Acceptor Unit: (a) cop3-BDT (b) cop3-diF2T (c) cop3-NDT (d) cop3-TT

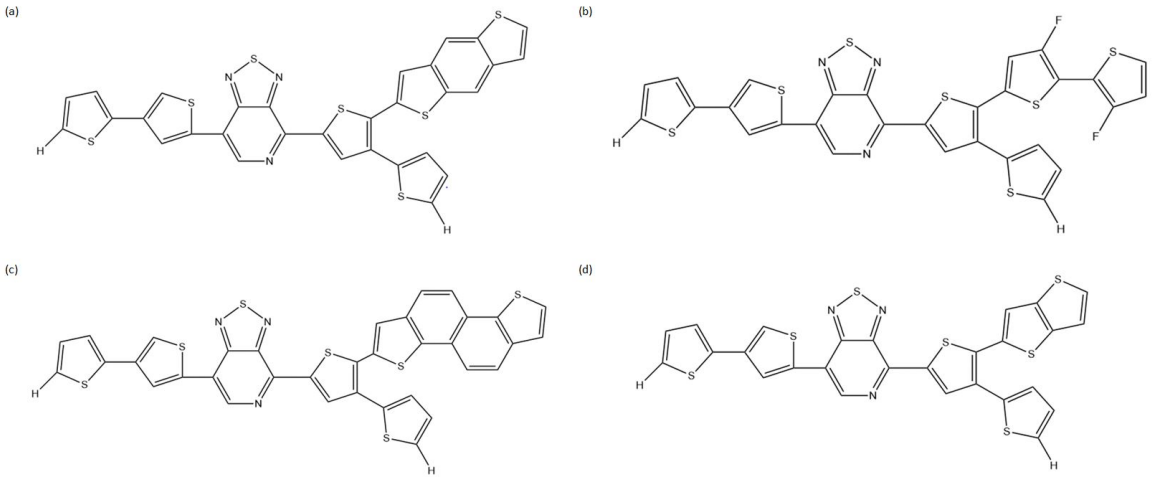

Figure 4.19. Structures of Molecules with cop4 as the Acceptor Unit: (a) cop4-BDT (b) cop4-diF2T (c) cop4-NDT (d) cop4-TT

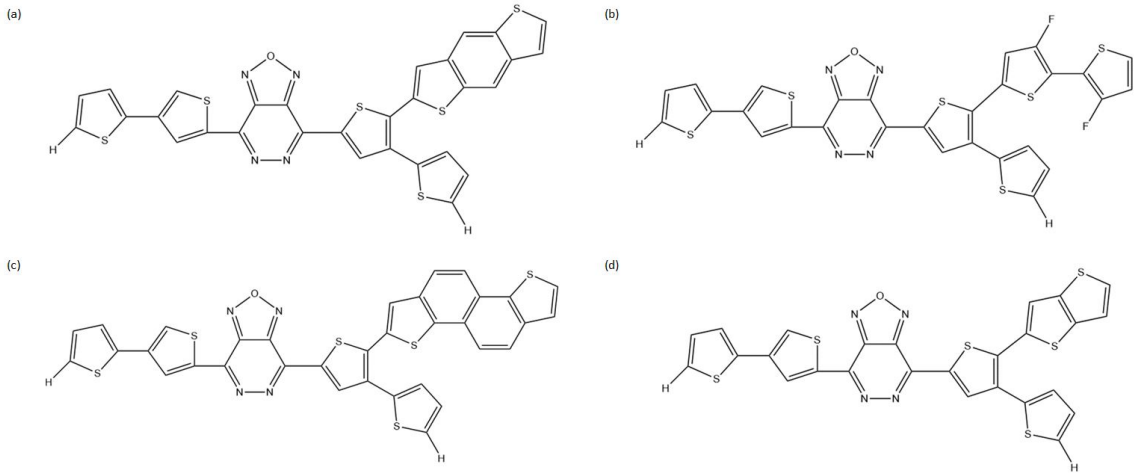

Figure 4.20. Structures of Molecules with cop5 as the Acceptor Unit: (a) cop5-BDT (b) cop5-diF2T (c) cop5-NDT (d) cop5-TT

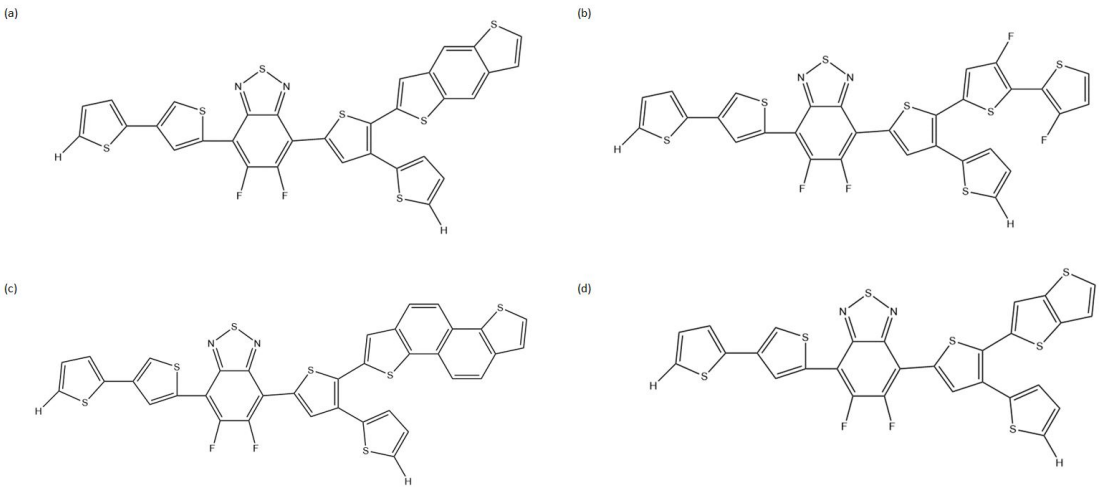

Figure 4.21. Structures of Molecules with FBTz as the Acceptor Unit: (a) FBTz-BDT (b) FBTz-diF2T (c) FBTz-NDT (d) FBTz-TT

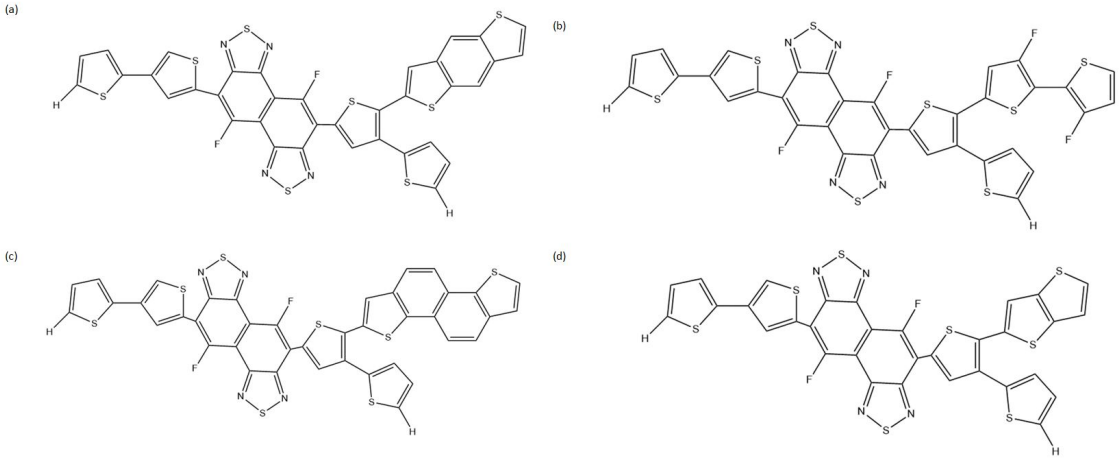

Figure 4.22. Structures of Molecules with FNTz as the Acceptor Unit: (a) FNTz-BDT (b) FNTz-diF2T (c) FNTz-NDT (d) FNTz-TT

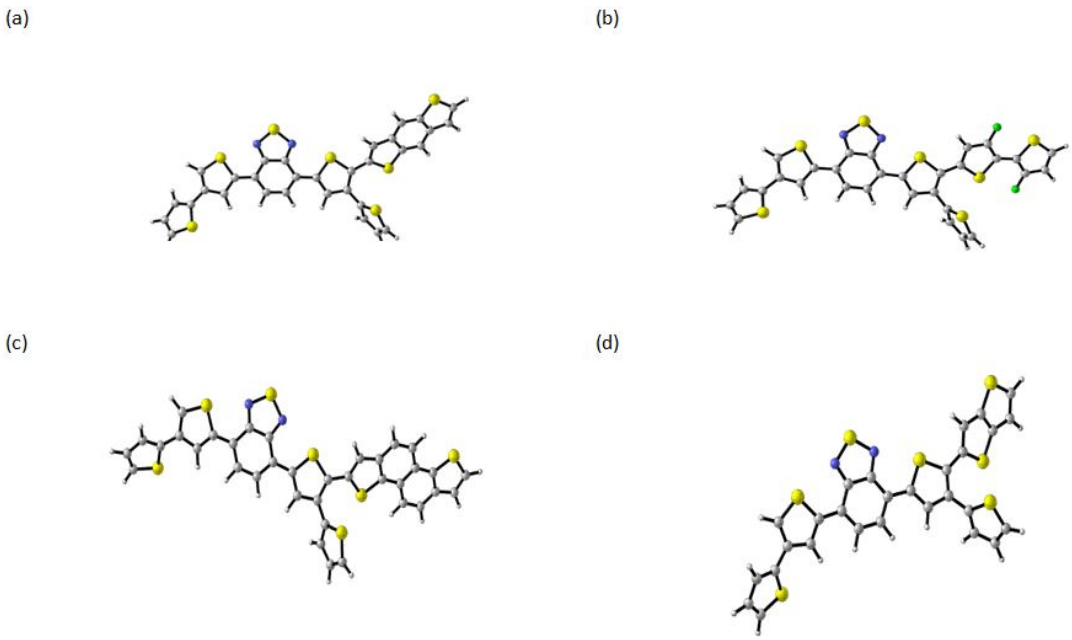

Figure 4.23. 3D Structures of (a) cop1-BDT (b) cop1-diF2T (c) cop1-NDT (d) cop1-TT

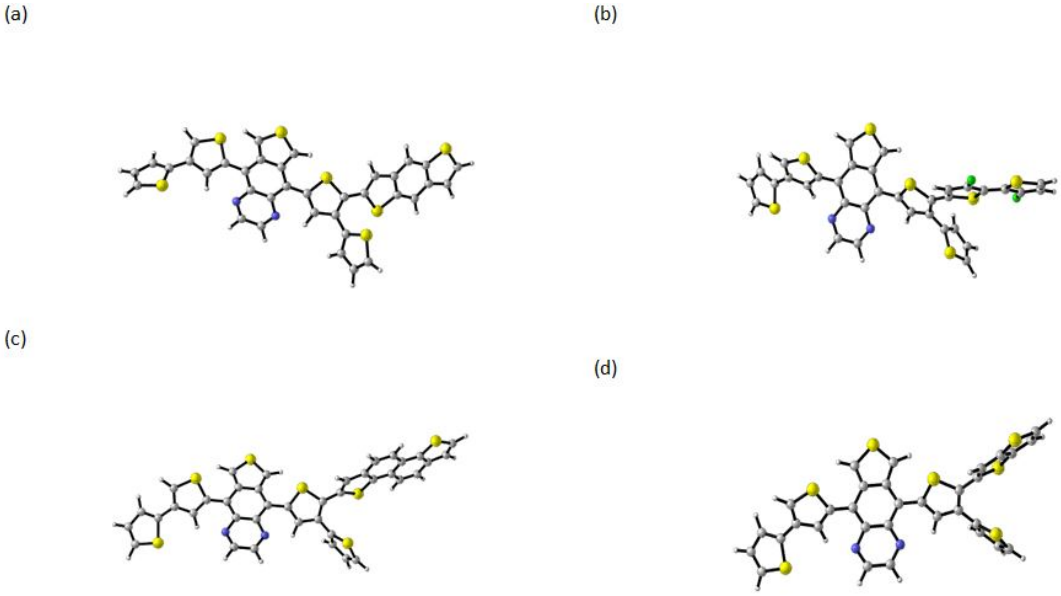

Figure 4.24. 3D Structures of (a) cop2-BDT (b) cop2-diF2T (c) cop2-NDT (d) cop2-TT

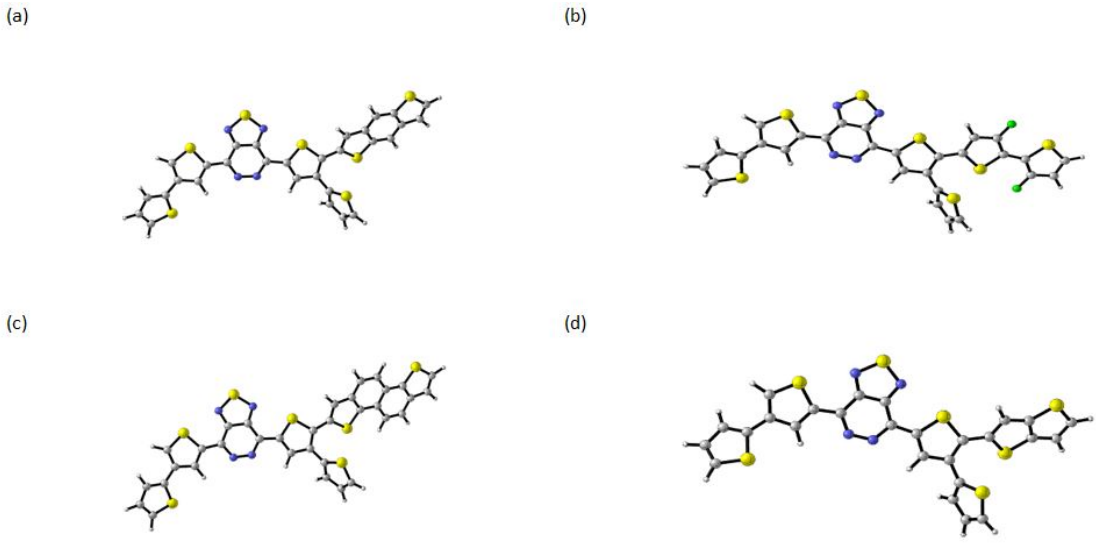

Figure 4.25. 3D Structures of (a) cop3-BDT (b) cop3-diF2T (c) cop3-NDT (d) cop3-TT

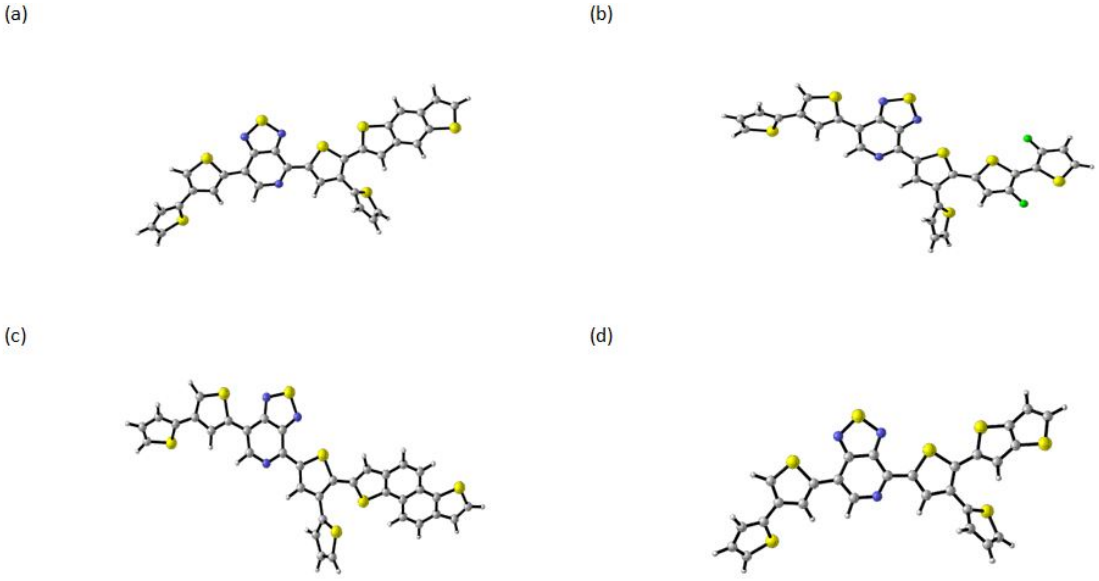

Figure 4.26. 3D Structures of (a) cop4-BDT (b) cop4-diF2T (c) cop4-NDT (d) cop4-TT

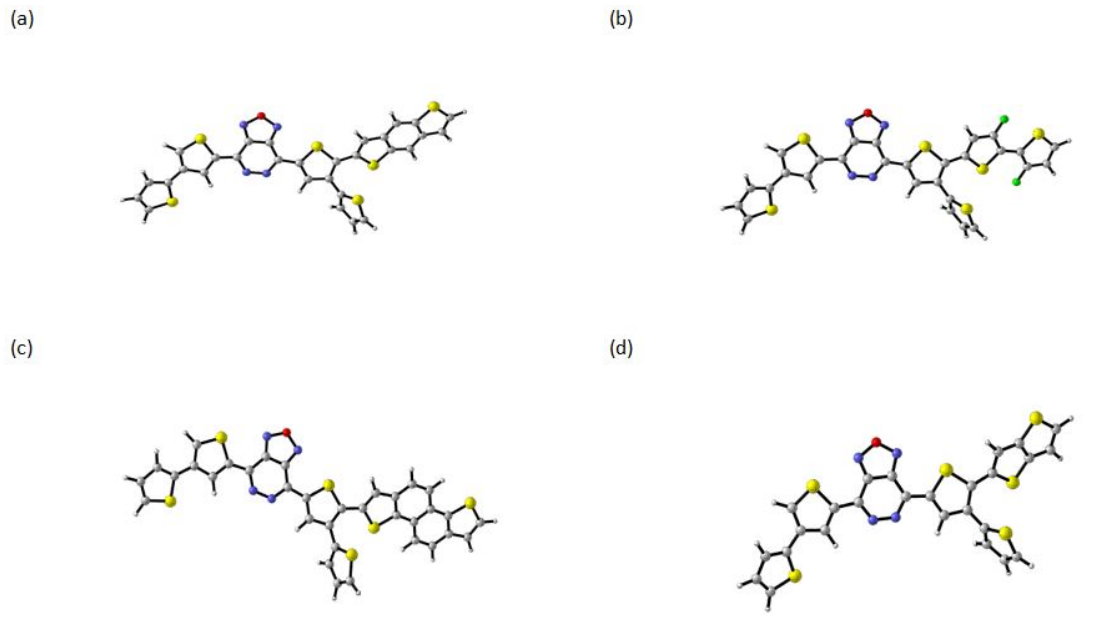

Figure 4.27. 3D Structures of (a) cop5-BDT (b) cop5-diF2T (c) cop5-NDT (d) cop5-TT

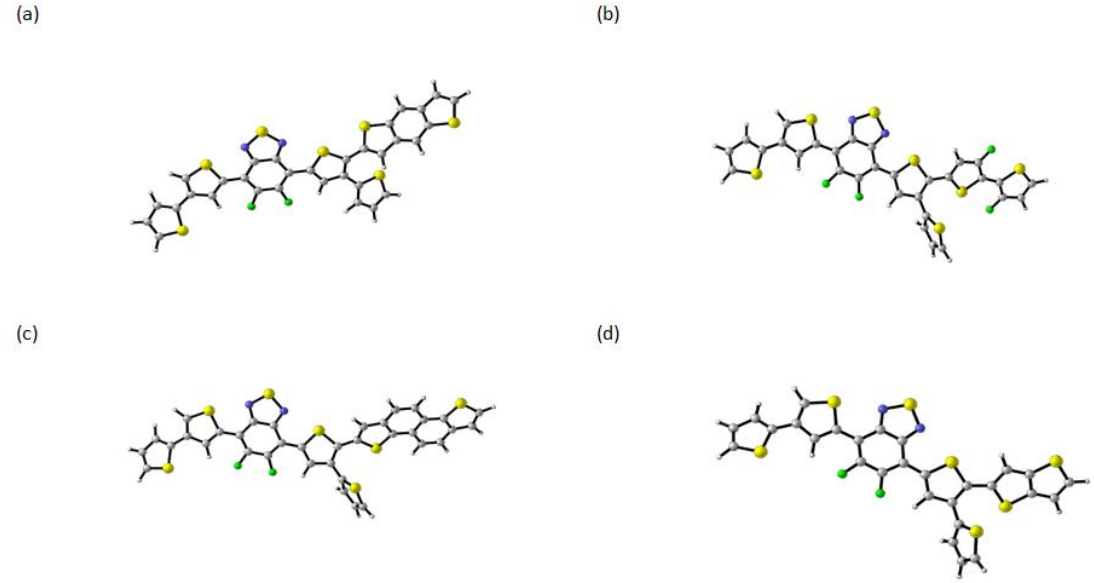

Figure 4.28. 3D Structures of (a) FBTz-BDT (b) FBTz-diF2T (c) FBTz-NDT (d) FBTz-TT

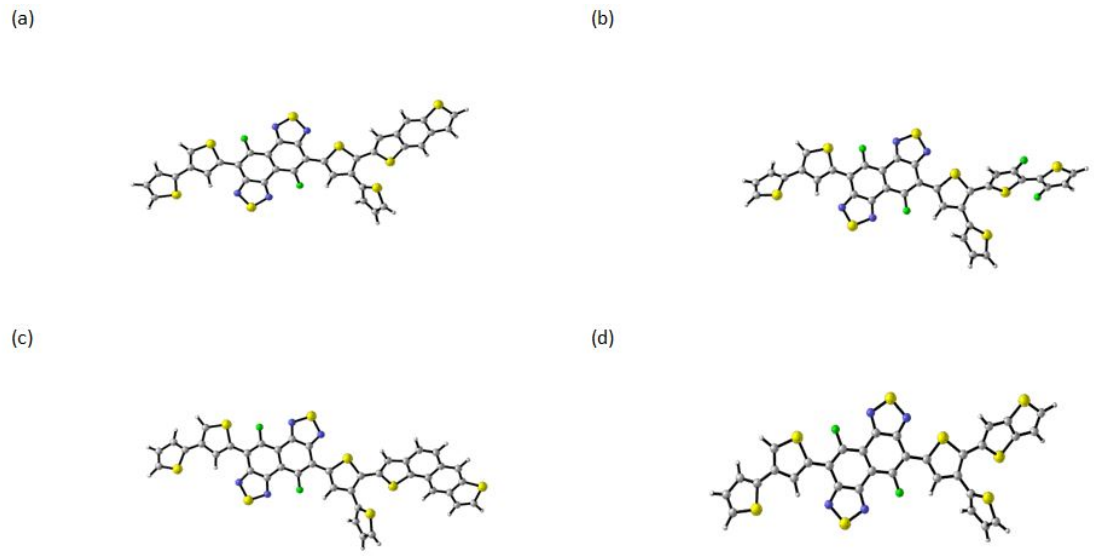

Figure 4.29. 3D Structures of (a) FNTz-BDT (b) FNTz-diF2T (c) FNTz-NDT (d) FNTz-TT

Table 4.15. HOMO, LUMO and E_g Values for Molecules Under Investigation, Neutral Ground State (B3LYP/6-311G*) (eV)

Name	**HOMO**	**LUMO**	**Eg**
COP1-BDT	-5.40	-2.97	2.42
COP1-diF2T	-5.32	-3.00	2.32
COP1-NDT	-5.39	-2.97	2.42
COP1-TT	-5.29	-3.09	2.20
COP2-BDT	-5.27	-2.98	2.30
COP2-diF2T	-5.27	-2.99	2.27
COP2-NDT	-5.31	-2.97	2.35
COP2-TT	-5.31	-2.96	2.36
COP3-BDT	-5.58	-3.47	2.12
COP3-diF2T	-5.51	-3.47	2.03
COP3-NDT	-5.59	-3.45	2.14
COP3-TT	-5.60	-3.44	2.17
COP4-BDT	-5.44	-3.22	2.22
COP4-diF2T	-5.43	-3.24	2.19
COP4-NDT	-5.50	-3.22	2.28
COP4-TT	-5.45	-3.19	2.26
COP5-BDT	-5.67	-3.55	2.12
COP5-diF2T	-5.62	-3.55	2.06
COP5-NDT	-5.69	-3.53	2.16
COP5-TT	-5.72	-3.52	2.20
FBTz-BDT	-5.52	-3.09	2.43
FBTz-diF2T	-5.43	-3.12	2.30
FBTz-NDT	-5.50	-3.10	2.40
FBTz-TT	-5.49	-3.07	2.42
FNTz-BDT	-5.50	-3.40	2.10
FNTz-diF2T	-5.64	-3.42	2.22
FNTz-NDT	-5.43	-3.39	2.05
FNTz-TT	-5.50	-3.38	2.12

Table 4.16. HOMO, LUMO and E_g Values for Molecules Under Investigation, Reduced State (PBE0/6-311G*) (eV)

Name	**HOMO**	**LUMO**	**Eg**
COP1-BDT	-2.75	-1.11	1.65
COP1-diF2T	-2.71	-1.14	1.58
COP1-NDT	-2.76	-1.10	1.66
COP1-TT	-2.63	-0.97	1.66
COP2-BDT	-2.49	-1.31	1.18
COP2-diF2T	-2.47	-1.31	1.16
COP2-NDT	-2.47	-1.27	1.21
COP2-TT	-2.37	-1.17	1.20
COP3-BDT	-3.09	-1.44	1.65
COP3-diF2T	-3.03	-1.47	1.56
COP3-NDT	-3.07	-1.44	1.63
COP3-TT	-3.00	-1.33	1.67
COP4-BDT	-2.87	-1.29	1.58
COP4-diF2T	-2.85	-1.32	1.53
COP4-NDT	-2.89	-1.30	1.59
COP4-TT	-2.83	-1.14	1.68
COP5-BDT	-3.16	-1.55	1.61
COP5-diF2T	-3.09	-1.58	1.51
COP5-NDT	-3.14	-1.55	1.59
COP5-TT	-3.06	-1.44	1.62
FBTz-BDT	-2.72	-1.06	1.66
FBTz-diF2T	-2.89	-1.25	1.65
FBTz-NDT	-2.95	-1.21	1.74
FBTz-TT	-2.83	-1.09	1.74
FNTz-BDT	-3.21	-1.59	1.62
FNTz-diF2T	-3.18	-1.61	1.58
FNTz-NDT	-3.20	-1.58	1.62
FNTz-TT	-2.92	-1.21	1.71

4.2.3. Distortion Energies

Benchmark values for distortion energy are in between 3.08 and 7.03 kcal/mol. And the molecules which satisfy HOMO, LUMO, E_g value and distortion energy benchmark are FBTz-NDT, FBTz-TT and FNTz-TT. Table 4.29 displays the dihedral angles and distortion energies of all molecules under investigation.

4.2.4. Reorganization Energies

The calculated energies show the reorganization energies for hole vary in between 255 and 342 meV whereas the reorganization energies for electron are in between 281 and 306 meV. The molecules satisfying HOMO, LUMO, E_g values, distortion energies and reorganization energies are FBTz-NDT and FBTz-TT. Table 4.30 demonstrates the reorganization energies of hole and electron, AIP, AEA, VIP and VEA values for all molecules under investigation.

4.2.5. Selection of Suitable Molecules

There are six important criteria which are HOMO, LUMO, optical band gap, distortion energy, reorganization energy for holes and reorganization energy for electrons in order to determine suitable molecules in organic solar cells.

First, HOMO values of the molecules should be in between -5.38 and -5.46 eV. Second, LUMO values should be in between -2.59 and -2.67 eV. Third, optical band gaps should be in between 1.78 and 1.91 eV. Fourth, distortion energies should vary in between 3.08 and 7.03 kcal/mol. And finally, reorganization energies for hole vary in between 255 and 342 meV whereas reorganization energies for electron should be in between 281 and 306 meV.

The molecules satisfying the conditions above are selected as suitable molecules for organic solar cells which are FBTz-NDT and FBTz-TT.

Table 4.17. Dihedral Angles and Distortion Energies in kcal/mol of Studied Molecules

Molecules	ϕ_1	ϕ_2	ϕ_3	ΔE_{tot}
COP1-BDT	40.69	-11.94	13.81	5.73
COP1-diF2T	13.53	-10.03	29.79	1.86
COP1-NDT	-5.38	-3.64	41.73	9.73
COP1-TT	-13.91	-9.49	40.47	5.45
COP2-BDT	46.86	-47.60	43.06	22.70
COP2-diF2T	-48.01	45.56	33.38	17.59
COP2-NDT	-47.55	47.24	45.47	23.36
COP2-TT	-47.87	46.77	51.24	27.48
COP3-BDT	0.43	-2.51	40.74	5.94
COP3-diF2T	0.56	-1.40	27.02	1.28
COP3-NDT	0.37	-2.40	40.65	5.79
COP3-TT	-0.26	-1.94	40.25	5.47
COP4-BDT	-30.57	1.16	-16.68	3.86
COP4-diF2T	-16.48	1.46	-30.87	3.81
COP4-NDT	-16.19	-1.88	40.17	5.62
COP4-TT	-32.75	1.47	-16.86	4.54
COP5-BDT	38.58	-3.29	0.71	4.96
COP5-diF2T	0.56	-1.96	25.08	1.03
COP5-NDT	0.64	-3.05	38.74	4.87
COP5-TT	36.00	-3.15	0.64	3.72
FBTz-BDT	-57.38	9.74	-3.93	4.39
FBTz-diF2T	-8.29	-3.18	28.91	1.60
FBTz-NDT	-5.38	-3.13	39.57	5.12
FBTz-TT	-8.61	-4.84	38.39	4.46
FNTz-BDT	0.90	-9.52	41.17	6.04
FNTz-diF2T	-0.46	8.78	69.06	2.23
FNTz-NDT	-1.26	-9.82	42.82	6.79
FNTz-TT	-1.69	-6.41	39.47	4.92

Table 4.18. Reorganization Energies for Hole and Electron and AIP, AEA, VIP and VEA Values for Studied Molecules

Molecules	λ_{Hole}	$\lambda_{Electron}$	**AIP**	**AEA**	**VIP**	**VEA**
COP1_BDT	332.82	282.45	6.18	-1.95	6.38	-1.77
COP1_DİF2T	344.20	260.38	6.13	-1.98	6.33	-1.83
COP1_NDT	418.69	269.21	6.05	-1.95	6.34	-1.78
COP1_TT	376.99	254.44	6.18	-1.86	6.41	-1.72
COP2_BDT	386.36	417.04	6.06	-2.00	6.25	-1.79
COP2_DİF2T	394.51	391.99	6.03	-2.02	6.26	-1.81
COP2_NDT	407.83	391.99	6.03	-1.99	6.28	-1.77
COP2_TT	465.28	383.30	6.06	-1.92	6.35	-1.73
COP3_BDT	322.76	252.12	6.39	-2.35	6.57	-2.21
COP3_DİF2T	332.64	234.96	6.34	-2.36	6.53	-2.24
COP3_NDT	324.06	246.91	6.34	-2.33	6.53	-2.20
COP3_TT	2003.31	237.44	6.41	-2.28	6.63	-2.16
COP4_BDT	266.60	160.61	6.28	-2.06	6.41	-2.02
COP4_DİF2T	333.73	157.13	6.24	-2.09	6.43	-2.04
COP4_NDT	336.68	258.68	6.23	-2.16	6.44	-2.00
COP4_TT	334.73	179.72	6.29	-1.97	6.47	-1.96
COP5_BDT	314.69	2041.65	6.50	-2.30	6.69	-2.30
COP5_DİF2T	329.68	245.03	6.46	-2.46	6.65	-2.33
COP5_NDT	317.43	256.67	6.46	-2.43	6.65	-2.29
COP5_TT	363.74	247.76	6.54	-2.37	6.75	-2.25
FBTZ_BDT	411.48	297.98	6.35	-2.13	6.58	-1.88
FBTZ_DİF2T	322.60	258.55	6.26	-2.09	6.44	-1.95
FBTZ_NDT	307.04	265.87	6.26	-2.06	6.44	-1.90
FBTZ_TT	345.59	255.18	6.31	-1.98	6.52	-1.85
FNTZ_BDT	285.97	172.16	6.25	-2.39	6.42	-2.31
FNTZ_DİF2T	3239.25	212.33	4.12	-2.55	6.55	-2.29
FNTZ_NDT	254.73	185.55	6.17	-2.38	6.33	-2.28
FNTZ_TT	946.61	175.99	5.69	-2.35	6.45	-2.26

Figures 4.30 and 4.31 show the natural transition orbitals for selected molecules. As benchmark molecules, the NTO analysis of FBTz-NDT and FBTz-TT shows that the distribution of electrons is denser around the donor parts in HOMO orbitals while the distribution of electrons is denser around the acceptor parts in LUMO orbitals.

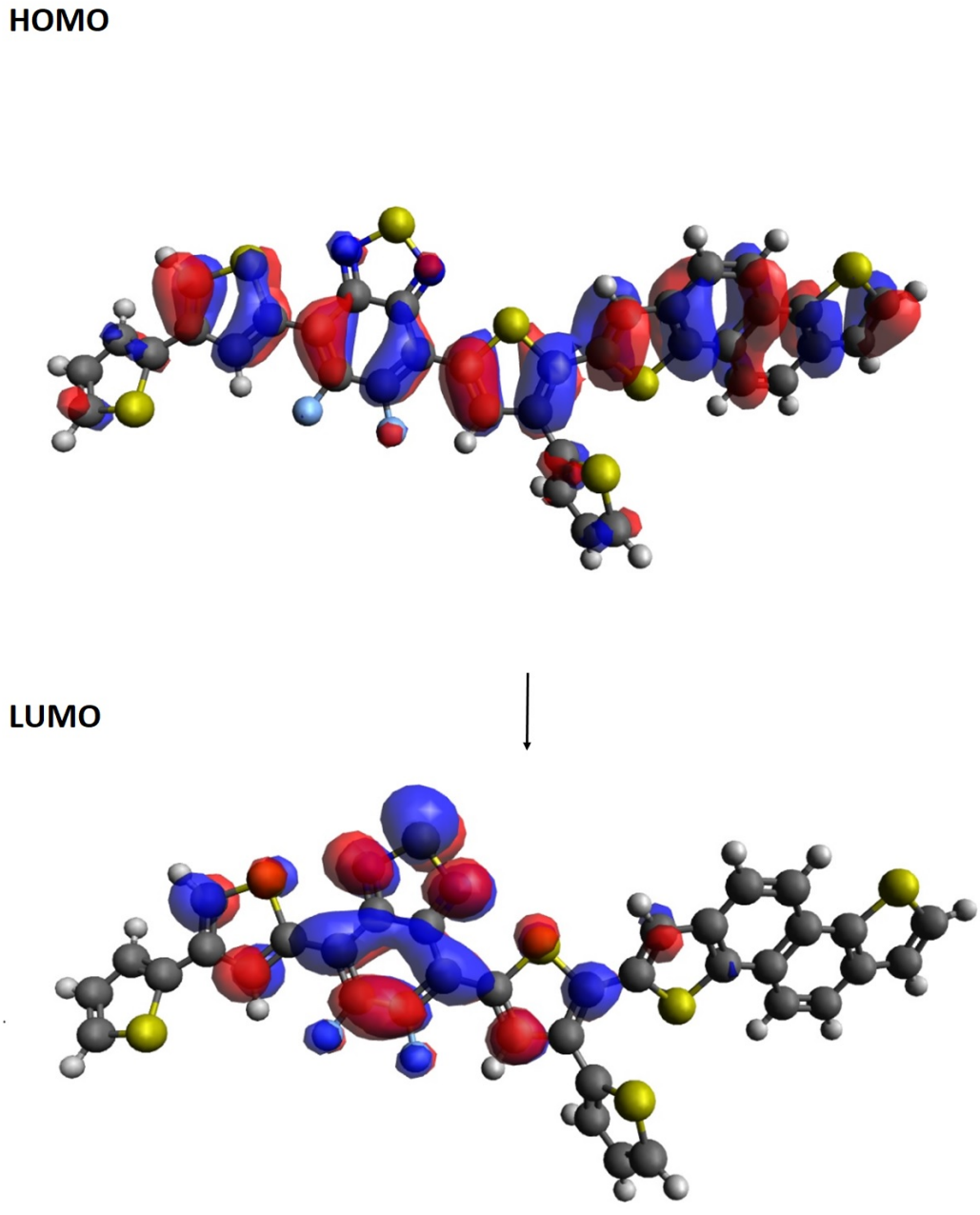

Figure 4.30. Natural Transition Orbitals of FBTz-NDT, B3LYP/6-311G*

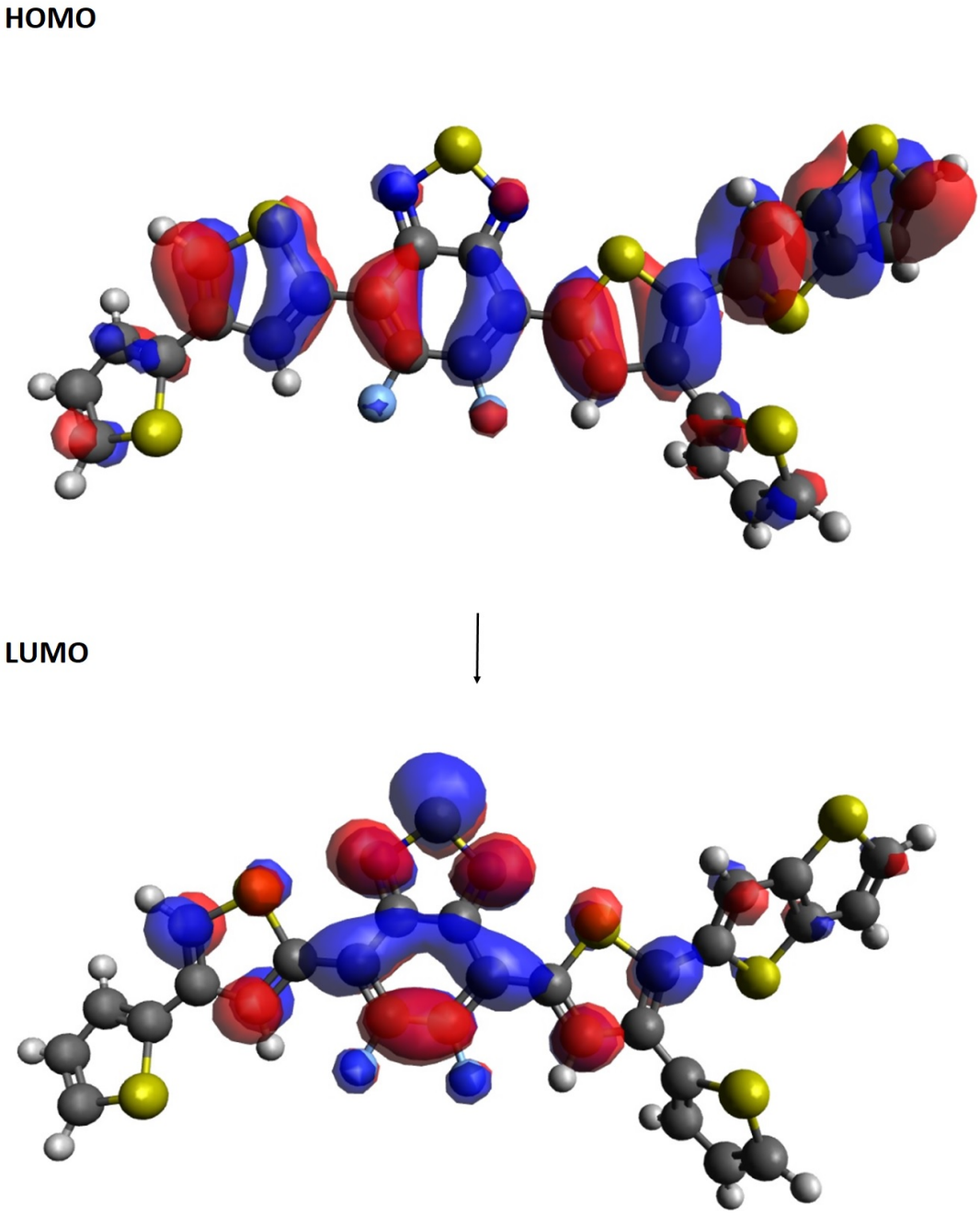

Figure 4.31. Natural Transition Orbitals of FBTz-TT, B3LYP/6-311G*

5. CONCLUSION

Geometric and optical properties of a group of donor-acceptor conjugated polymers in order to receive high-performing organic cell molecules were investigated computationally. Four different donors and one acceptor and these four different donors were combined with seven different acceptors in order to create effective molecules for high-performing organic solar cells. Thanks to benchmark calculations which contain five different models and four different functionals including B3LYP, ωB97XD, PBE0 and M06-2X with 6-311G* as basis set, HOMO, LUMO energies and optical band gaps were calculated and as a result, accurate calculations were performed with the correct methodology. It was found that the best functional predicting HOMO and LUMO energies is B3LYP in neutral-ground state and the best functional predicting the optical energy band gap is PBE0 in reduced state.

2 molecules were determined as suitable materials out of 28 molecules according to six important criteria which contain electron transfer reorganization energy range between 281 meV and 306 meV, hole transfer reorganization energy range between 255 meV and 342 meV, distortion energy range between 3.08 kcal/mol and 7.03 kcal/mol, LUMO energy range between -2.59 eV and -2.67 eV, HOMO energy range between -5.38 eV and -5.46 eV, and the optical band gap between 1.78 eV and 1.98 eV. In this study, the donors of NDT and TT, combining with the acceptor FBTz have shown the best performance.

REFERENCES

1. Mehta, A., A. Kapoor and H. K. Neopaney, "Conceptual Design of Concentrated Solar Power Plant using SPT- Solar Power Tower Technology", , 2014.

2. Bagher, A. M., "Rational Design of High Performance Conjugated Polymers for Organic Solar Cells", *Macromolecules*, Vol. 45, pp. 607–632, 2012.

3. Seferos, D. S., T. M. McCormick, C. R. Bridges, E. I. Carrera, P. M. Dicarmine, G. L. Gibson, J. Hollinger and L. M. Kozycz, "Conjugated Polymers: Evaluating DFT Methods for More Accurate Orbital Energy Modeling", *Macromolecules*, Vol. 46, No. 10, pp. 3879–3886, 2013.

4. BP, *1965-2017 BP Statistical Review of World Energy*, 2017, `http://www.columbia.edu/ mhs119/EnergyConsump/`.

5. Gheorge, A. V., Bostan, Dulgheru, Sobor, Bostan and Sochirean, "Resilient Energy Systems Renewables: Wind, Solar, Hydro", *Springer Dordrecht Heidelberg New York London*, 2013.

6. Kamat, P. V., "Meeting the Clean Energy Demand: Nanostructure Architectures for Solar Energy Conversion", *The Journal of Physical Chemistry C*, Vol. 111, No. 7, pp. 2834–2860, 2007.

7. Miles, R. W., G. Zoppi and I. Forbes, "Inorganic Photovoltaic Cells", *Materialstoday*, Vol. 10, No. 11, pp. 20–27, 2007.

8. Mekemeche, A., M. Beghdad, M. Belarbi, B. Semmache and Y. Cuminal, "Two Dimensional Device Simulation and Performance Optimization of n-type Silicon Solar Cell Structure Using PC2D", *Solar Energy*, Vol. 146, pp. 119–124, 2017.

9. Salavei, A., D. Menossi, F. Piccinelli, A. Kumar, G. Mariotto, M. Barbato,

M. Meneghini, G. Meneghesso, S. D. Mare, E. Artegian and A. Romeo, "Comparison of High Efficiency Flexible CdTe Solar Cells on Different Substrates at Low Temperature Deposition", *Solar Energy*, Vol. 139, pp. 13–18, 2016.

10. Moradi, M., R. Teimouri, M. Saadat, M. Zahedifar, G. Mariotto, M. Barbato, M. Meneghini, G. Meneghesso, S. D. Mare, E. Artegian and A. Romeo, "Buffer Layer Replacement: A Method for Increasing The Conversion Efficiency of CIGS Thin Film Solar Cells", *Optik*, Vol. 136, pp. 222–227, 2017.

11. Che, H., X. Liu, Y. Gao, J. Liu and Z. Cao, "Hydrothermal Electrochemical Deposition Synthesis $NiSe_2$ as Efficient Counter Electrode Materials for Dye-Sensitized Solar Cells", *Journal of Alloys and Compounds*, Vol. 705, pp. 645–651, 2017.

12. Lin, W. K., S. Su, M. C. Yeh, C. Y. Chen and M. Yokoyama, "Enhancing Efficiency of Perovskite Solar Cells Using a Thin Buffer Layer", *Vacuum*, Vol. 140, pp. 82–88, 2017.

13. Bagher, A. M., "Comparison of Organic Solar Cells and Inorganic Solar Cells", *International Journal of Renewable and Sustainable Energy*, Vol. 3, pp. 53–58, 2014.

14. Liu, X., R. He, W. Shen and M. Li, "Molecular Design of Donor-Acceptor Conjugated Copolymers Based on C-, Si- and N-bridged Dithiophene and Thienopyrroledione Derivatives Units for Organic Solar Cells", *Journal of Power Sources*, Vol. 245, pp. 217–223, 2014.

15. Bagher, A. M., "Introduction to Organic Solar Cells", *Sustainable Energy*, Vol. 2, No. 3, pp. 85–90, 2014.

16. Bauerle, P. and A. Mishra, "Small Molecule Organic Semiconductors on the Move: Promises for Future Solar Energy Technology", *Angewandte Chemie International Edition*, Vol. 51, No. 9, pp. 2020–2067, 2012.

17. Scharber, M. C., D. Muhlbacher, M. Koppe, P. Denk, C. Waldauf, A. J. Heeger and C. J. Brabec, "Design Rules for Donors in Bulk Hetero-Junction Solar Cells Towards 10% Energy-Conversion Efficiency", *Advanced Materials*, Vol. 18, pp. 789–794, 2006.

18. Brabec, C. J., N. S. Sariciftci and J. C. Hummelen, "Plastic Solar Cells", *Advanced Functional Materials*, Vol. 11, No. 1, pp. 15–26, 2001.

19. Liu, Z., Q. Liu, Y. Huang, Y. Ma, S. Yin, X. Zhang, W. Sun and Y. Chen, "Organic Photovoltaic Devices Based on a Novel Acceptor Material: Graphene", *Advanced Materials*, Vol. 20, pp. 3924–3930, 2008.

20. Gunes, S., H. Neugebauer and N. S. Sariciftci, "Conjugated Polymer-Based Organic Solar Cells", *Chemical Reviews*, Vol. 107, pp. 1324–1338, 2007.

21. He, M., W. Li, H. Tian, H. Tong, J. Zhang, J. Liu, Y. Gang and F. Wang, "Wide Band-Gap Donor-Acceptor Conjugated Polymers with Alkylthiophene as Side Chains for High-Performance Non-Fullerene Polymer Solar Cells", *Organic Electronics*, Vol. 65, pp. 31–38, 2019.

22. Mestiri, T. and K. Alimi, "DFT and TD-DFT Design of Small π-Conjugated Molecules with Narrow Band Gap and High Efficiency for Organic Solar Cells", *Theoretical Chemistry Accounts*, Vol. 137, No. 133, 2018.

23. Chatterjee, S., Y. Ie, T. Seo, T. Moriyama, G.-J. A. H. Wetzelaer, P. W. M. Blom and Y. Aso, "Fluorinated Naphtho[1,2-c:5,6-c']bis[1,2,5] Thiadiazole-Containing π-Conjugated Compound: Synthesis, Properties, and Acceptor Applications in Organic Solar Cells", *NPG Asia Materials*, Vol. 10, pp. 1016–1028, 2018.

24. Frisch, M. J., G. W. Trucks, H. B. Schleger, G. Scuseria, M. A. Robb, J. R. Cheeseman, G. Scalmani, V. Barone, B. Mennuci, G. A. Petersson, H. Nakatsuji, M. Caricato, X. Li, H. P. Hratchian, A. F. Izmaylov, J. Bloino, G. Zheng, J. L. Sonnenberg, M. Hada, M. Ehara, K. Toyota, R. Fukuda, J. Hasegawa, M. Ishida,

T. Nakajima, Y. Honda, O. Kitao, H. Nakai, T. Vreven, J. A. M. Jr., J. E. Peralta, F. Ogliaro, M. Bearpark, J. J. Heyd, E. Brothers, K. N. Kudin, V. N. Staroverov, R. Kobayashi, J. Normand, K. Raghavachari, A. Rendell, J. C. Burant, S. S. Iyengar, J. Tomasi, M. Cossi, N. Rega, N. J. Millam, M. Klene, J. E. Knox, J. B. Cross, V. Bakken, C. Adamo, J. Jaramillo, R. Gomperts, R. E. Stratmann, O. Yazyev, A. J. Austin, R. Cammi, C. Pomelli, J. W. Ochterski, R. L. Martin, K. Morokuma, V. G. Zakrzewski, G. A. Voth, P. Salvador, J. J. Dannenberg, S. Dappriarch, A. D. Daniels, O. Farkas, J. B. Foresman, J. V. Ortiz, J. Cioslowski and D. J. Fox, *Gaussian 09 Revision D.01*, Wallingford CT, 2009.

25. Parl, R. G. and T.Weitao, *Density Functional Theory of Atoms and Molecules*, Oxford University Press, 1989.

26. Kohn, W. and L. J. Sham, "Self Consistent Equations Including Exchange and Correlation Effects", *Physical Review*, Vol. 140, pp. A1133–A1138, 1965.

27. Becke, A. D., "Density Functional Thermochemistry. III. The Role of Exact Exchange", *The Journal of Chemical Physics*, Vol. 98, pp. 5648–5652, 1993.

28. Zhao, Y. and D. G. Truhlar, "The M06 suite of density functionals for main group thermochemistry, thermochemical kinetics, noncovalent interactions, excited states, and transition elements: two new functionals and systematic testing of four M06-class functionals and 12 other functionals", *Theoretical Chemistry Accountss*, Vol. 120, pp. 215–241, 2008.

29. ucla.edu, *Conformational Energy Searching*, `https://c125.chem.ucla.edu/NIH/conformati`

30. Pandey, L., C. Risko, J. E. Norton and J.-L. Bredas, "Donor−Acceptor Copolymers of Relevance for Organic Photovoltaics: A Theoretical Investigation of the Impact of Chemical Structure Modifications on the Electronic and Optical Properties", *Macromolecules*, Vol. 45, pp. 6405–6414, 2012.

31. Coropceanu, V., J.Cornil, D. A. Filho, Y. Olivier, R. Silbey and J. L. Bredas,

"Charge Transport in Organic Semiconductors", *Chemical Reviews*, Vol. 107, No. 4, pp. 926–952, 2007.

32. Oshi, R., S. Abdalla and M. Springborg, "Study of The Influence of Functionalization on The Reorganization Energy of Naphthalene Using DFT", *Computational and Theoretical Chemistry*, Vol. 1099, pp. 209–215, 2017.

33. Martin, R. L., "Natural Transition Orbitals", *The Journal of Chemical Physics*, Vol. 118, pp. 4775–4777, 2003.